MODELLING OF HELICAL COIL STEAM GENERATOR OF MOTEL FACILITY WITH COMPUTATIONAL FLUID DYNAMICS (CFD) CODE

SAfe and REliable Nuclear Applications SARENA program (Nuclear Reactors Operation and Safety NROS track)

Lappeenranta–Lahti University of Technology (LUT)
LUT School of Energy Systems
Master's Programme in Energy Technology, Nuclear Engineering

University of Ljubljana
Faculty of Mathematics and Physics
Nuclear Engineering

Lappeenranta, 2023

Tokzhan Toleukaiyr

Supervisors: Assist. Prof. Ivo Kljenak/ Giteshkumar Patel, D.Sc. [Tech.]

Examiner(s): Prof. Juhani Hyvärinen

Assist. Prof. Ivo Kljenak

ABSTRACT

Lappeenranta–Lahti University of Technology LUT/ University of Ljubljana UL
School: LUT School of Energy Systems/Faculty of Physics and Mathematics UL
Degree program: SARENA joint degree program

Tokzhan Toleukaiyr

Modelling of helical coil steam generator of MOTEL facility with Computational Fluid Dynamics (CFD) code

Master's thesis
2023
59 pages, 33 figures, 8 tables, and 1 appendix
Examiner(s): Prof. Juhani Hyvärinen and Assist. Prof. Ivo Kljenak

Keywords: Small Modular Reactors, helical coil steam generator, heat transfer, boiling

The MOTEL test facility is a model of an integral pressurized water small modular reactor that runs on natural circulation, and it is located at LUT University, Finland. The MOTEL facility has a steam generator with a helical coil and a generic core rod bundle. The facility is used to conduct thermal-hydraulic experiments and to provide data for the validation of safety analysis tools such as subchannel codes, computational fluid dynamics (CFD) codes, and thermal-hydraulic system codes.

In this thesis, the ANSYS Fluent CFD code has been used to model a single helical coil and helical coil immersed in a cylindrical pool to investigate the effectiveness of the system. The Volume of Fluid (VOF) method with an implicit scheme, the Lee model and a user-defined function for mass transfer have been utilized for the simulation. The used turbulence model is the $k-\varepsilon$ model with standard wall functions as it has been extensively used in the literature.

The results suggest that all the simulated cases are comparable to each other. For the different boundary conditions, the outlet temperature of the coil was in the range of 463-473 K, the velocity was between 30 and 40 m/s, and the liquid-water volume fraction was between 0.148 and 0.2. Finally, the future research directions are suggested.

ACKNOWLEDGEMENTS

I would like to extend my sincere gratitude to the examiners, Prof. Juhani Hyvärinen and Assist. Prof. Ivo Kljenak, for their guidance and support throughout my master's thesis work. I also wish to express my special appreciation to my dedicated supervisors, Assist. Prof. Ivo Kljenak and Giteshkumar Patel, D.Sc. [Tech.], for their invaluable help and support during the entire thesis process.

Furthermore, I am deeply thankful to Prof. Juhani Vihavainen for introducing me to the topic and delivering insightful lectures during the second semester at LUT. I would also like to acknowledge the entire staff who actively participated in the SARENA program and provided support during my two-year master's journey.

I reserve special thanks to my family and younger brother, Zhandaulet, who consistently believed in me and supported my educational pursuit abroad.

My appreciation goes to my friends from SARENA and those who shared the academic journey with me at IMT Atlantique University. Lastly, I'd like to express my separate gratitude to the friends who stood by me during the thesis writing phase at LUT.

SYMBOLS AND ABBREVIATIONS

Roman characters

C	specific heat	[J/kg·K]
d	tube diameter	[m]
D	coil diameter	[m]
E	energy	[J/kg]
$\vec{F}$	external body force	[N/m^3]
$h_{j,q}$	heat transfer coefficient	[W/m^2]
k	turbulence kinetic energy	[J/kg]
k_{eff}	effective thermal conductivity	[W/(m·K)]
p	pressure	[Pa]
q_m	mass flow rate	[kg/s]
R	gas constant	[J/kg K]
S_m	source term	[kg/ (m^3· s)]
T	temperature	[K]
t	time	[s]
u	velocity in x-direction	[m/s]
u'	fluctuating in velocity x-direction	[m/s]
$\bar{u}$	mean velocity in x-direction	[m/s]
U	velocity magnitude	[m/s]
v	velocity vector	[m/s]
V	volume	[m^3]

Greek characters

α	incidence angle	[°]
δ_{ji}	Kronecker delta	[NA]
ε	turbulence dissipation rate	[m^2/s^3]
$\bar{\bar{\tau}}$	stress tensor	[Pa, N/m^3]
v	kinematic viscosity	[m^2/s]
λ	thermal conductivity	[W/mK]
μ	dynamic viscosity	[Pa·s]
ρ	density	[kg/m^3]

Constants

g	gravitational acceleration	9,81 m/s^2

Dimensionless quantities

Re	Reynolds number
x	vapour content

Abbreviations

BWR	Boiling Water Reactor
CFD	Computational Fluid Dynamics
CHT	Conjugate Heat Transfer
GVF	Gas Volume Fraction
HTGR	High-Temperature Gas-cooled Reactor
IAEA	International Atomic Energy Agency

LUT	Lahti-Lappeeranta University of Technology
LWR	Light Water Reactor
MASLWR	Modular Advanced Small Light Water Reactor
MOTEL	Modular Test Loop
MR	Microreactor
MSR	Molten Salt Reactor
NPP	Nuclear Power Plant
PWR	Pressurized Water Reactor
RANS	Reynolds-Averaged Navier-Stokes
SG	Steam Generator
SMR	Small Modular Reactor
SST	Shear Stress Transport Model
UDF	User Defined Function
VOF	Volume of Fluid

Table of contents

Abstract

Acknowledgements

Symbols and abbreviations

1 Introduction 5
1.1 Thesis aim and organization 7
1.2 Motivation of the thesis 8
2 Literature review 9
2.1 Small Modular Reactors 9
2.2 Studies on helical coil steam generators of SMRs 11
3 A general view of the MOTEL facility 13
3.1 Structure of MOTEL 13
3.2 Helical coil steam generator of MOTEL test facility 16
4 Computational fluid dynamics (CFD) 20
4.1 Governing equations 20
4.2 Multiphase Flow Model 22
4.3 Turbulence models 23
4.3.1 The $k-\varepsilon$ model 25
4.4 Evaporation-Condensation Model 27
5 Methodology 28
5.1 Development of the single helical coil steam generator geometry (case-1) 29
5.2 The helical coil steam generator immersed in a cylindrical pool (case-2) 30
5.3 General setup for both cases 31
5.3.1 Simulation setup for case-1 with boundary conditions 32
5.3.2 Simulation setup for case-2 with boundary conditions 33
5.4 Mesh and convergence study for case-1 34
Convergence study using Mesh 3 37
6 Results and discussion 38
6.1 Results of the simulation for case-1 (Mesh 3) 38

6.1.1 Analysis of the results for case-1 41
6.2 Results of the simulation for case-2 at 463 K and 473 K pool inlet temperatures 44
6.2.1 Results at 463 K temperature 44
6.2.2 Results at the 473 K temperature 48
6.2.3 Analysis of the results for case-2 50
7 Conclusion 54
References 57

Appendices

Appendix 1. The UDF code

Figures

Figure 1. MOTEL facility general view on the left, main external parts in the middle and internal structures on the right 14
Figure 2 Left: steam generator pipes and collectors; right: water flow paths in the primary side ... 15
Figure 3. Whole construction on the left and view from the top of the helical coil steam generator on the right 17
Figure 4. Top view of the formed loop of the steam generator (left) and steam manifold (right) ... 18
Figure 5. The steam generator module 19
Figure 6. The geometry of the helical coil steam generator 29
Figure 7. The helical coil steam generator in a cylinder 30
Figure 8. Generated mesh for the pool and helical coil tube 31
Figure 9. Flow chart of preprocessing 32
Figure 10. Single helical coil mesh 36
Figure 11. Convergence study 37
Figure 12. Temperature contour in helical coil tube (case-1) 38
Figure 13. Volume fraction of liquid water in helical coil tube (case-1) 39
Figure 14. Density distribution of liquid-gas mixture in helical coil tube (case-1) 40
Figure 15. Velocity profile in helical coil tube (case-1) 41
Figure 16. Axial temperature profile of the helical coil tube (case-1) 42
Figure 17. Axial density profile of the liquid-gas mixture (case-1) 42
Figure 18. Axial volume fraction profile of the liquid water (case-1) 43
Figure 19. Axial velocity profile of the liquid-gas mixture (case-1) 43
Figure 20. Temperature profile of the helical coil in a cylindrical pool at inlet temperature 463 K (case-2) 44
Figure 21. Distribution of temperature in helical tube at pool inlet temperature 463 K (case-2) 45
Figure 22. Volume fraction of the liquid water at pool inlet temperature 463 K (case-2) 46
Figure 23. Density of liquid-gas mixture at pool inlet temperature 463 K (case-2) 47
Figure 24. Velocity of liquid-gas mixture at pool inlet temperature 463 K (case-2) 47
Figure 25. Temperature distribution in helical tube at pool inlet temperature 473 K (case-2) 48
Figure 26. Volume fraction of the liquid water at pool inlet temperature 473 K (case-2) 49
Figure 27. Density of liquid-gas mixture at pool inlet temperature 473 K (case-2) 49
Figure 28. Velocity of liquid-gas mixture at pool inlet temperature 473 K (case-2) 50
Figure 29. Axial temperature profiles of the helical coil for pool inlet temperatures 463 K and 473 K (case-2) 51
Figure 30. Axial volume fraction profiles of helical coil for pool inlet temperatures 463 K and 473 K (case-2) 51
Figure 31. Axial density profiles of liquid-gas mixture for pool inlet temperatures 463 K and 473 K (case-2) 52
Figure 32. Axial velocity profiles of liquid-gas mixture (case-2) 53
Figure 33. A comparison of the temperature profiles of case-1 and case-2 (pool inlet temperature 473 K) 53

Tables

Table 1: Examples of SMR reactor types 10
Table 2: Characteristics of the MOTEL test facility 15
Table 3: Parameters of the helical coil steam generator 19
Table 4: Pool and helical coil mesh description 31
Table 5: The used boundary conditions for single helical coil 33
Table 6: Boundary conditions for the case-2 34
Table 7: Single helical coil mesh comparison 35
Table 8: Mesh independence study results 36

1 Introduction

The increasing demands of a growing population, the effects of globalization, and the rise of urbanization contribute to the significance of energy as an indispensable necessity for sustaining daily activities and driving human and economic advancement worldwide. According to the International Atomic Energy Agency (IAEA), in 2019, the global electricity production surpassed 26,000 terawatt-hours, which relied on various energy sources including fossil fuels, nuclear power, and renewable sources such as solar, hydro, and wind (Jawerth, 2020). The production and consumption of energy represent the primary contributor to greenhouse gas emissions on a global scale. Since greenhouse gases play a significant role in driving climate change, countries across the world are actively engaged in transitioning towards clean energy by altering their methods of energy production (Jawerth, 2020). The transition towards clean energy involves a fundamental shift in energy production away from sources that emit substantial amounts of greenhouse gases, such as fossil fuels. Instead, the focus is on utilizing energy sources that release minimal to no greenhouse gases. Some examples of these clean energy sources include nuclear power, hydroelectricity, wind power, and solar energy.

Nuclear power is the second-largest source of low-carbon energy used for electricity generation today, following only hydropower. Nuclear power plants emit very little greenhouse gas while operating. According to the International Energy Agency, nuclear power usage has decreased more than 60 gigatonnes of CO_2 emissions during the last 50 years, equivalent to over two years' worth of global energy-related emissions (Jawerth, 2020).

When the term "nuclear power" is mentioned, it typically evokes images of large-scale power plants with towering cooling structures. However, the landscape of nuclear power is undergoing a transformation with the emergence of small modular reactors (SMRs) and microreactors (MRs) that are gradually becoming a tangible reality. This shift is reshaping the perception and scope of nuclear power. Small Modular Reactors could be part of the future energy-mix to achieve the low-carbon power generation goals with low key risk and cost in a competitive energy market. Thus, the general interest on the development and deployment of SMRs has increased in the last years worldwide. The first configuration of

the new Modular Test Loop (MOTEL) test facility at LUT has been designed for SMR-specific experiments. With the essential components including the helical coil steam generator, the core and the pressurizer modules stacked on top of each other to form a compact test loop operating with natural circulation, it closely resembles the design of the NuScale's SMR. The main idea of the facility is to be able to model any reactor model system configuration due to the unique modular design and construction which has exchangeable main components that are replaceable to similar ones with different designs. The MOTEL facility is used in the McSAFER (2020-2024) (Tielinen, 2021) project which is a three-year project funded by Euratom with the cooperation of 13 research organizations, to explore thermal-hydraulic phenomena that are unique to SMRs and to obtain data for the validation of safety analysis tools such as thermal-hydraulic system codes, subchannel codes, and codes that solve the basic equations of fluid mechanics on the local instantaneous scale (so-called Computational Fluid Dynamics (CFD) codes).

A reliable computational fluid dynamics software program called ANSYS Fluent enables accurate simulation of fluid flow, heat transport, and other physical processes. It will help to infer the detailed operation of the system and pinpoint areas for optimization and improvement by simulating the behaviour of a helical coil steam generator. Namely, although the results of CFD simulations will never be a perfect reproduction of real phenomena, it may safely be assumed that validated CFD codes reproduce the alleged phenomena, including the cause-and-effect relationships, with sufficient accuracy (Sanchez-Espinoza, 2021).

Due to its small size and effective heat transfer properties, the helical coil steam generator is a popular design for producing steam. And it is an essential component of the SMR, as it converts the heat generated by the reactor into steam that is used to drive a turbine and generate electricity. Helical coil steam generators are a promising option for SMRs due to their compact design and high efficiency. However, because of the complex flow patterns and heat transfer processes involved, creating and optimizing this kind of steam generator could be difficult (Huang, 2020).

1.1 Thesis aim and organization

The objective of this master's thesis is to model the operation of the helical coil steam generator of the MOTEL facility on the local instantaneous scale. For this, the CFD code ANSYS Fluent will be used. The simulation includes modelling the fluid flow and heat transfer within the steam generator as well as analyzing the influence of different operating conditions on the efficiency of the system.

This thesis has the following objectives:

- This thesis will conduct a literature survey on the available works concerning experiments and simulations of helical coil steam generator flows.
- Adequate grid generation will be done for MOTEL's helical coil steam generator geometry.
- A set of different simulations will be done considering heat-transfer modelling.

The following contents of the chapter go as:

The opening section of the thesis provides an extensive overview of the global energy landscape, emphasizing the role of nuclear energy. It also introduces small modular reactors (SMRs) as a cost-effective, low-carbon energy solution and underscores the pivotal role of the Modular Test Loop (MOTEL) facility, known for its modular design and participation in the McSAFER project, in advancing SMR research. Furthermore, it outlines the thesis's structure, objectives, and concludes by underscoring the significance of helical coil steam generators in SMRs and the thesis's goals.

- The section 2 of this thesis contains a brief summary of the studies on small modular reactors, with an emphasis on helical coil steam generators. It includes important research papers and technical reports that explore topics including design, performance, safety, and simulations utilizing CFD codes.
- The section 3 describes the MOTEL facility general structure with its dimensions and functions of the components. In subsection 3.2 discusses physical parameters of the helical coil steam generator, which includes dimensions and working principles.
- The section 4 provides information about models used in the simulation and their governing equations. Moreover, it explains the underlying theories related to the

turbulence model, specifically the $k-\varepsilon$ model and the pressure-based Volume of Fluid model.

- The section 5 of this thesis focuses on ANSYS Fluent simulation of the helical coil steam generator. Creating a three-dimensional model of part of the steam generator, establishing the fluid flow and heat transfer boundary conditions, and running the simulation to get data on the system's performance are all part of the simulation. Furthermore, it provides mesh independence and convergence study results.
- The section 6 of this thesis shows the simulation results and examines the influence of various operating circumstances on the performance of the simulated part of the steam generator. This involves an evaluation of heat transfer efficiency, temperature distribution and overall system performance.
- Lastly, it concludes overall thesis work, which has been done. Also, includes future work could be done for further investigation.

In summary, the goal of this master thesis is to advance the development of helical coil steam generators for small modular reactors and to provide valuable insights into their performance and operation within the MOTEL facility. The findings of this study could prove beneficial in enhancing the design and performance of future helical coil steam generators, as well as optimizing the operation of existing SMRs.

The assumptions and simplifications made during the modelling process, as well as the limitations of the ANSYS Fluent software in accurately capturing all the complex flow patterns and heat transfer processes involved in the operation of the helical coil steam generator, are among the limitations of this study.

1.2 Motivation of the thesis

It is common for boiling secondary flow to move through the inside of steam generator tubes in integral SMR applications, while primary coolant typically flows over the outside of the tubes. This setup is designed to optimize pressure drops in the primary coolant loop, allowing for maximum natural convection flow and heat elimination in case of an accident. As a result, it is crucial to thoroughly investigate the flows of helical coil steam generators, either through experiments or numerical simulations.

2 Literature review

This chapter provides a brief survey of the literature on small modular reactors focusing on the helical coil steam generators. It summarizes key research studies, technical publications, and reports on the design, performance, safety, and simulations using CFD codes. The purpose of this review is to provide a comprehensive summary of current knowledge and major results relevant to small modular reactors.

2.1 Small Modular Reactors

Small Modular Reactors (SMRs) represent a new generation of nuclear reactor designs that offer several advantages over conventional large-scale reactors. Here are some additional points about SMRs (WNA, 2023):

Modular Design: SMRs are designed with a modular approach, which means they can be constructed and assembled in a factory or a centralized location. These modules can then be transported to the deployment site, providing flexibility in installation and reducing on-site construction time and costs.

Scalability: SMRs are characterized by their lower power output, typically up to 300 MWe per unit. This scalability allows for incremental capacity additions, enabling more flexibility in meeting energy demands and grid requirements. Multiple SMR units can be deployed together to achieve the desired power output.

Enhanced Safety Features: SMRs incorporate advanced safety features to ensure reliable and secure operations. Their smaller size inherently enhances safety by reducing the potential consequences of accidents. Furthermore, some SMR designs utilize passive safety systems, which rely on natural processes like gravity and natural convection to cool the reactor in case of emergencies.

Flexibility in Deployment: The compact size of SMRs makes them suitable for various applications and deployment scenarios. They can be utilized in remote areas, providing power to off-grid communities or industrial operations. SMRs also offer potential

applications in desalination, heat generation for industrial processes, or serving as a complement to renewable energy sources.

Improved Economics: SMRs have the potential to provide more favourable economics compared to large-scale reactors. The modular design reduces upfront capital costs, and the ability to manufacture components in a controlled environment improves construction quality and efficiency. Additionally, the scalability allows for phased investments based on electricity demand growth.

Advanced Technologies: SMRs encompass a range of advanced reactor technologies, including small pressurized water reactors (PWRs), high-temperature gas-cooled reactors (HTGRs), molten salt reactors (MSRs), and more. These technologies often incorporate innovative fuel designs, improved efficiency, and advanced materials to enhance performance and sustainability.

It's important to note that while SMRs offer several advantages, their deployment and widespread adoption are still an ongoing process. Various SMR designs are under development, with some already in operation or undergoing regulatory review. The specific characteristics and benefits may vary depending on the individual SMR design (WNA, 2023). The SMRs can be of different designs, as it is shown in Table 1.

Table 1: Examples of SMR reactor types (IAEA, 2020).

Name of design	**Cooling type**	**Power, [MWe]**
ARC-100 (Canada)	liquid sodium	100
BWRX-300 (USA)	boiling water reactor	300
eVinciTM (USA)	solid core heat pipe	25
IMSR (USA)	integral molten salt reactor	200
MMR-5, MMR-10 (USA)	high temperature gas	5-10
Moltex Energy Stable Salt Reactor (Canada)	molten salt	300
NuScale (USA)	integral pressurized water reactor	60
SEALER (Sweden)	molten lead	3
SMR-160 (USA)	pressurized water reactor	160
StarCore Module (Canada)	high temperature gas	10
The Nuward	pressurized water reactor	300-400
U-Battery (Canada)	high temperature gas	4
Xe-100 (USA)	high temperature gas	75

Additionally, due to their small size, the amount of radioactive material is planned to be smaller than in large-scale reactors, which is beneficial in case of unlikely radioactive release and for the spent fuel management. The underground or underwater deployment of the SMRs is planned, resulting in higher resilience to the man-made or natural hazards (WNA, 2023).

2.2 Studies on helical coil steam generators of SMRs

The steam generator (SG) plays a crucial role in ensuring the safety of nuclear power plants, making its reliability a critical concern. Over the years of operation, a considerable amount of steam generators have experienced failures or defects, leading to their removal from service or necessitating repairs (Yuan, 2017).

Helical coil steam generators are gaining significant attention in SMR designs due to their compact size and high heat transfer efficiency. The helical coil design allows for efficient steam production and is a crucial component in converting reactor heat into electricity (Huang, 2020).

Several studies have utilized computational fluid dynamics (CFD) simulations, specifically using ANSYS Fluent, to investigate the fluid flow and heat transfer characteristics within helical coil steam generators. These simulations enable a detailed analysis of the complex flow patterns and thermal behavior, providing valuable insights into the performance and optimization of the system (Lai, 2016). The simulation of helical coil steam generators using ANSYS Fluent involves the creation of a three-dimensional model, specifying appropriate boundary conditions, and solving the governing equations for fluid flow and heat transfer. The simulations can capture important parameters such as pressure drop, temperature distribution, and heat transfer coefficients, allowing for a comprehensive evaluation of the system's performance.

Researchers have used ANSYS Fluent simulations to investigate the effect of various operating conditions on the performance of helical coil steam generators. These conditions include inlet steam properties, coolant flow rates, geometric parameters, and different design configurations. The simulations provide a valuable tool for optimizing the system's performance and identifying potential areas for improvement.

In 2002, Rennie and Raghavan modelled the properties of heat transport in a double tube heat exchanger. They demonstrated that the heat exchanger's overall heat transfer coefficient can be limited by the flow in the inner tube. The overall heat transfer coefficient will rise as other variables are stabilized (Rennie, 2002). Similarly, Ranjbar and Seyyedvalilu in 2014 conducted a CFD analysis of a helical coil steam generator, focusing on both geometric and operational factors and validated with experimental results in the open literature. Their work emphasized the significance of accurate boundary conditions; however, they highlighted that the results of the simulation are independent from meshing techniques. They pointed that with increasing the inner tube diameter, curvature ratio and decreasing the pitch of the heat exchanger coil would help to increase efficiency of the heat transfer (Ranjbar, 2014).

In 2017, Jaffar et al. used ANSYS Fluent software to investigate the temperature distribution along the length and radial direction as well as the flow velocity within a helical coil heat exchanger. The study focused on the effect of centrifugal forces on heat transfer efficiency and pressure drop characteristics considering the unique design of tube. The findings emphasized the importance of accurate boundary conditions and the proper application of correlations in order to provide reliable simulations. Furthermore, the study proved that CFD simulation may be used to design and understand the various internal phenomena of an efficient helical coil heat exchanger (Jaffar, 2017).

Another notable study by Che, Breitenmoser et al. (2020) employed CFD simulations to analyse the effects of helical coil geometry on heat transfer and pressure drop in a steam generator. The study showed the significance of proper meshing techniques and accurate boundary conditions for obtaining reliable results. They highlighted the advantages of helical coil configurations in terms of enhanced heat transfer and reduced pressure drop compared to conventional straight tube designs (Che1, 2020).

These studies show the relevance of CFD simulations for studying helical coil steam generators in general. They provided insight into how geometric parameters, operational settings, and design decisions affected heat transfer effectiveness and pressure drop properties. It will help to increase the efficiency of helical coil steam generators and improve system design by utilizing CFD techniques to maximize their performance.

3 A general view of the MOTEL facility

This chapter presents an overview of the facility, including its dimensions, overall characteristics and basic properties. Then it focuses on the helical coil steam generator's description and working principle.

3.1 Structure of MOTEL

The MOTEL is developed at LUT University, Nuclear Engineering Laboratory as a multifunctional integral test facility to study thermal-hydraulic phenomena and nuclear safety features. The design resembles MASLWR (Modro, 2003) and NuScale (Reyes, 2012) reactor designs with a tall cylindrical reactor vessel presented in Figure 1 (Hyvärinen, 2022). The MOTEL reactor vessel primary side consists of (Tielinen, 2021):

- a straight cylinder reactor core heated electrically at the bottom;
- a hot riser;
- a pressuriser at the top;
- an annular downcomer volume.

The secondary side of SMR model consists of:

- a water reservoir;
- a feedwater injection system;
- the helical coil system generator;
- a steam outlet system (Tielinen, 2021).

There is no containment, emergency core cooling and decay heat removal system due to cost considerations. The primary side system functions based on natural circulation, where the coolant rises through a central riser tube above the steam generator, flows downward via the steam generator located between the riser tube and the pressure vessel, and subsequently returns to the core through the downcomer (Kilchanov, 2022).

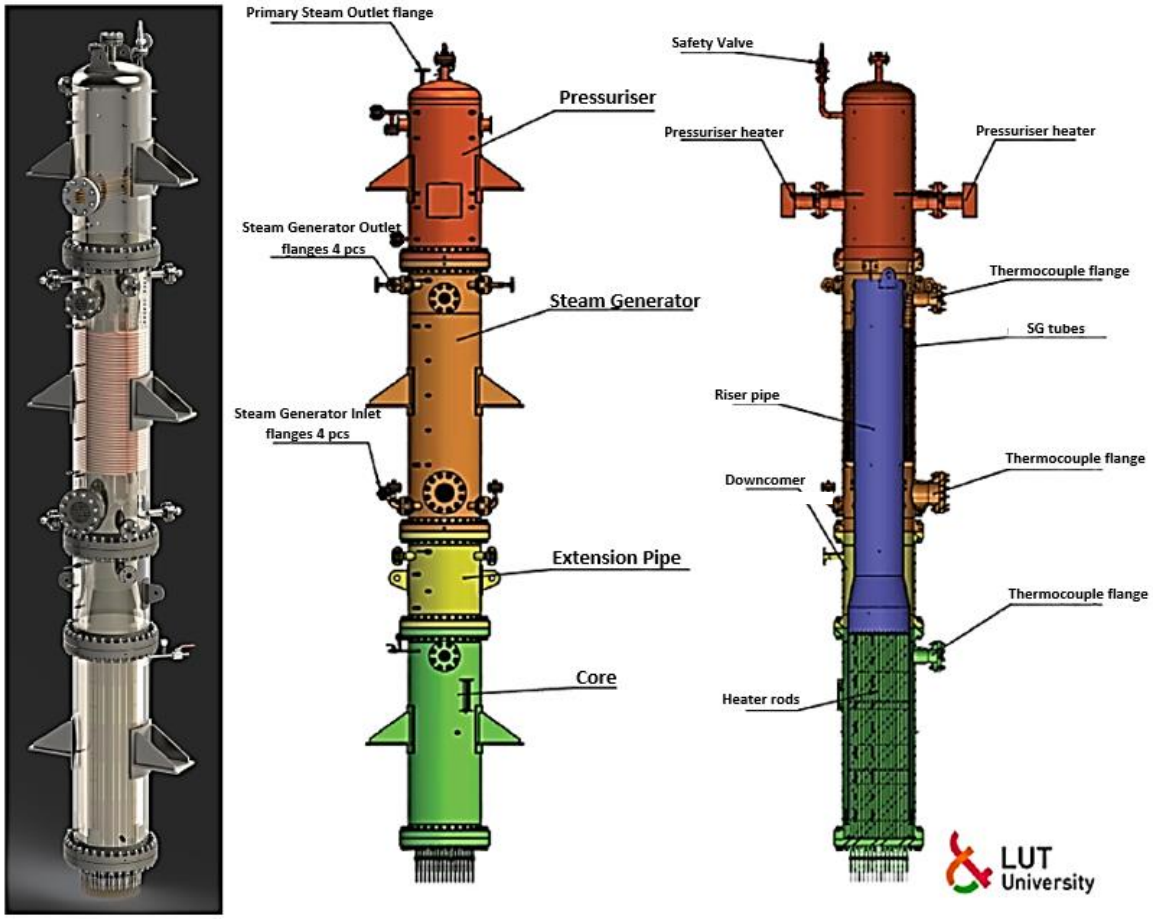

Figure 1. MOTEL facility general view on the left (Telkkä, 2018), main external parts in the middle and internal structures on the right (Telkkä, 2022).

The secondary side has a pump to inject the feedwater from the water reservoir via a water manifold to four cold water collectors. The water flow starts in the cold collectors and continues through the steam generator tubes. Each cold collector feeds four tubes with secondary water. The water within the tubes boils as it receives heat from the primary side. The produced steam is then directed to four heated collectors. Then it exits the pressure vessel via pipelines and eventually reaches a steam manifold before being released from the system (Tielinen, 2021). (See Figure 2 for a visual representation of the steam generator's structure and placement within the pressure vessel).

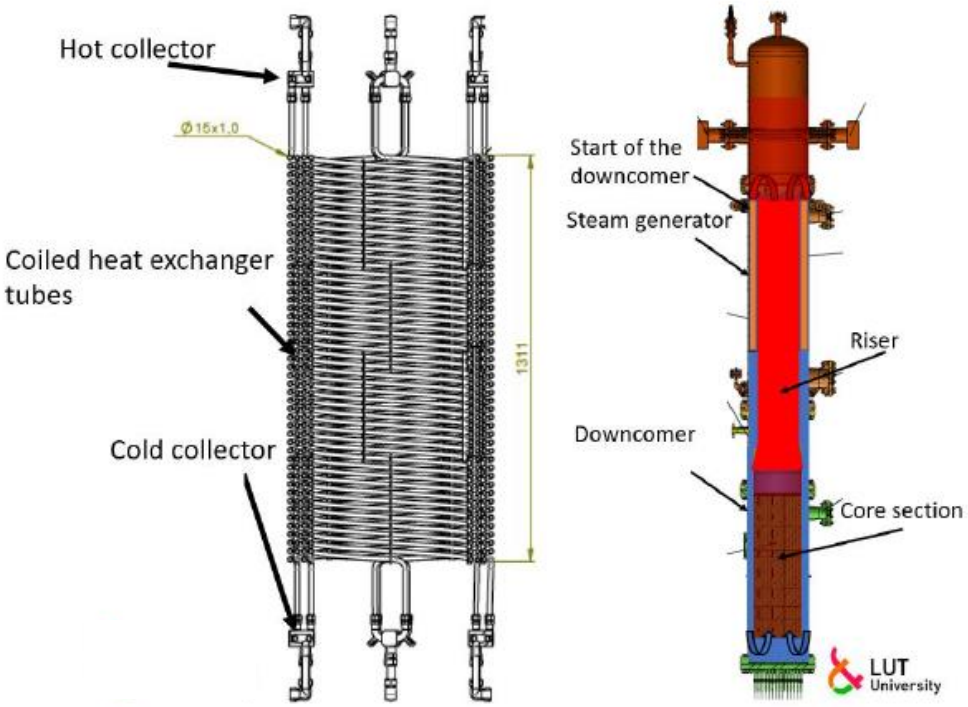

Figure 2 Left: steam generator pipes and collectors; right: water flow paths in the primary side (Tielinen, 2021).

The main characteristics of the MOTEL test facility are presented in Table 2.

Table 2: Characteristics of the MOTEL test facility (Tielinen, 2021).

Specifications	**Motel facility**
Total height [m]	7.4
Outside diameter of main vessel [mm]	711
Maximum primary/secondary pressure [bar]	40
Maximum primary/secondary temperature [°C]	250
Number of helical coil steam generator tubes	16
Maximum core heating power [kW]	990
Number of heater rods	132
Heated length of heater rods [mm]	1830
Diameter of heater and measurement rods [mm]	19.05
Number of measurement rods	16
Number of dummy rods	145
Diameter of dummy rods [mm]	18
Main material of the components	Stainless steel
Insulation material / thickness [mm]	Mineral wool / 120, aluminium cover

3.2 Helical coil steam generator of MOTEL test facility

The helical coil steam generator is an essential part of the MOTEL design. One distinguishing feature is that the primary side flow and boiling occur within the steam generating tubes. The secondary side water, on the other hand, flows through the pool side of the steam generator tube bundles outside the tubes (Telkkä, 2022). It is clear that the configuration of the system's geometry is primarily dictated by the specific application and other requirements. In such a system, the predominant mode of heat transfer is through conduction.

In terms of heat transfer efficiency, helical coil heat exchangers outperform straight tubes. This is mostly due to the coil's curved structure, which creates centrifugal forces on the fluid running through it, resulting in secondary flows. These secondary flows help to increase the heat transfer coefficient, improve mixing, and reduce frictional pressure drop, especially in laminar flow conditions. As a result, helical coil heat exchangers better than straight tubes in terms of heat transfer performance (Alkan, 2022).

The test facility is equipped with a helical coil steam generator comprising four bundles of heat exchange tubes. Each bundle consists of four tubes arranged in four radial layers, with two coils rotating in opposite directions (clockwise and half counterclockwise) and the bundle has its own hot and cold collector. The tube's diameter and length were chosen to closely resemble the prototype, within the limitations of commercially available tubes. The outer diameter is 15 mm with a wall thickness of 1 mm. The length of the pipes ranges from 20 to 25.1 m. The nominal gap between the layers of pipes is 7.5 mm, although slight variations may occur due to the curvature of the rolls not being perfectly uniform. There are four feedwater collectors, each supplying all four layers of tubular coils (four tubes in each layer) (Hyvärinen, 2022). The whole steam generator and plane view are shown in Figure 3.

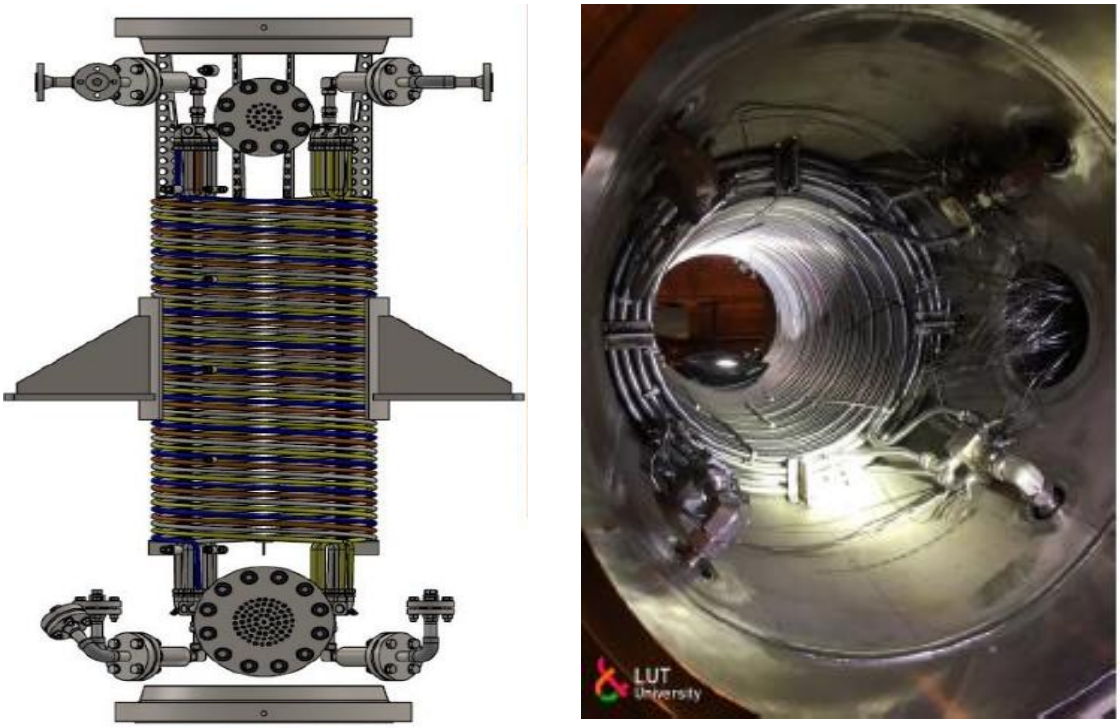

Figure 3. Whole construction on the left (Tielinen, 2021) and view from the top of the helical coil steam generator on the right (Telkkä, 2018).

Due to variations in length and coiling, the tubes of the steam generator of the MOTEL facility form loops with different diameters. Each loop contains four steam generator tubes arranged on four separate layers leading to variations in the diameters of the four loops, ranging from 515 mm to 650 mm. Figure 4 shows a visual representation of the loops and steam manifold in the steam generator of the MOTEL facility (Tielinen, 2021).

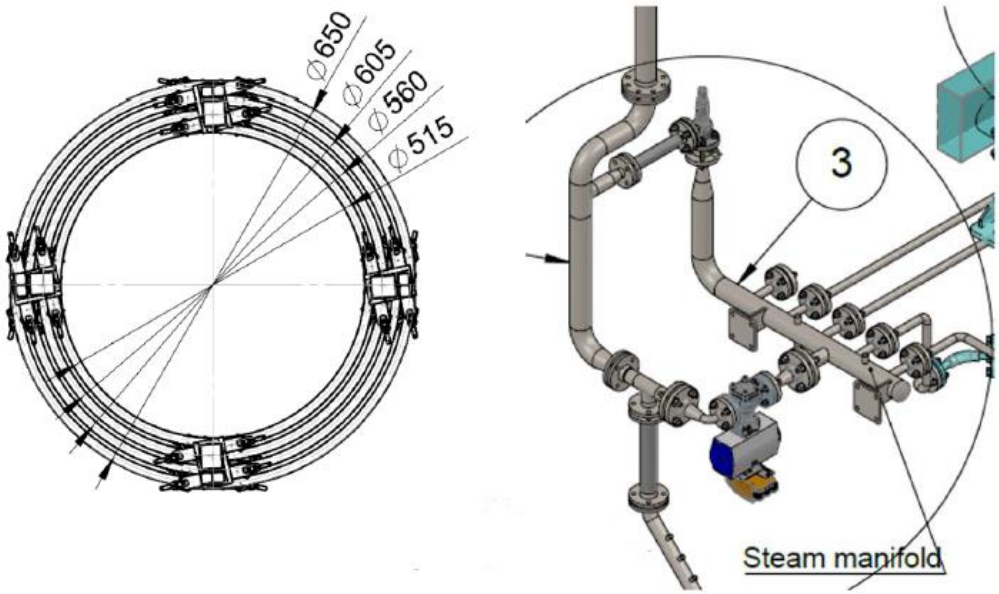

Figure 4. Top view of the formed loop of the steam generator (left) and steam manifold (right) (Tielinen, 2021).

On the secondary side, cold water is fed into the steam generating tubes via four cold collectors as shown in Figure 2. Each inlet pipe to the cold collectors has been equipped with a control valve that can be entirely closed. This allows for the isolation of specific steam generator tube bundles. Inside steam generator tubes, boiling occurs, resulting in the production of steam. The produced steam then goes to the hot collectors. Four steam pipelines transport the generated steam from the hot collectors and the pressure vessel to the steam manifold. This allows for the directed flow of steam from the hot collectors and pressure vessel to the centralized steam manifold (Telkkä, 2018).

The exterior wall of the steam generator module serves as the outer pool of the pressure vessel in the top section of the annular downcomer space. This is also where the bundles of steam generator tubes are located. Figure 5 depicts the steam generator module pool, which has a weight of 1163 kg. As can be seen from Figure 5 the steam generator is placed inside the steam generator module. In the pressure vessel of the MOTEL, it is located at the top of the annular downcomer space. The system of steam generation and effective heat transfer are both guaranteed by this placement. In order to provide effective insulation and containment of the produced steam, the steam generator module offers a dedicated space for the steam generator. Its placement within the annular downcomer space

optimizes coolant flow and improves the process's overall efficiency for producing steam (Telkkä, 2018).

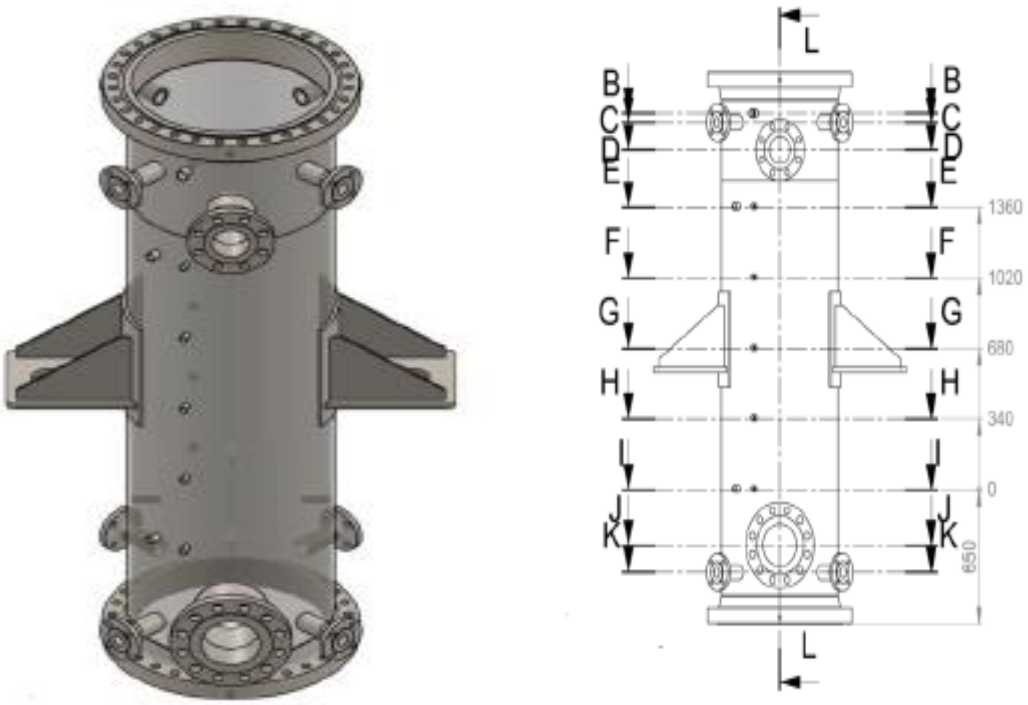

Figure 5. The steam generator module (Tielinen, 2021).

The main characteristics of the steam generator are listed in Table 3.

Table 3: Parameters of the helical coil steam generator (Kilchanov, 2022).

Characteristics	**Steam generator of the MOTEL**
Height of the helical coil steam generator [m]	1.311
Total amount of tubes / Number of layers	16 / 4
Tube outer diameter / wall thickness, [mm]	15 / 1
Tube lengths, [m]	20.0 / 21.7 / 23.4 / 25.1
Coil diameters, [mm]	515 / 560 / 605 / 650
Total heat transfer area, [m^2]	17
Tube material	Stainless steel

4 Computational fluid dynamics (CFD)

This section introduces the model used in the simulation, including the multiphase flow model, the interaction models, and the turbulence model. Moreover, it covers governing equations used in the CFD, which is basically the numerical solving of the equations on the local instantaneous scale.

4.1 Governing equations

In concept, conservation in fluid dynamics is simple, but it can be complicated internally. It states that internal sources and the amount crossing the border (flux) influence the change in a conserved flow quantity within a volume. Sources and flux depend on space-time coordinates and fluid motion. Conservation laws apply to mass, momentum, and energy, defining the evolution of fluid flows (Hirsch, 2007).

In the ANSYS Fluent code depending on the nature of the flow there are conservation equations that need to be solved (Ansys, 2021).

- For all flows, mass and momentum conservation equations are solved to describe fluid motion.
- When there is heat transfer involved, an additional equation for energy conservation is solved to consider the temperature variations.
- Transport equations are added for turbulent flows to capture turbulence effects, such as turbulence kinetic energy (k) and its dissipation rate (ε) for the $k-\varepsilon$ turbulence model.

The principle of mass conservation assures that the overall mass of fluid in the system remains constant over time. The continuity equation, which defines how the rate of change of fluid density is connected to the divergence of the fluid velocity field, describes this principle (Anderson, 2020).

- General form of the mass conservation equation for incompressible flow is given below (Ansys, 2021):

$$\frac{\partial \rho}{\partial t} + \nabla \cdot (\rho \vec{u}) = S_m \tag{1}$$

where ρ fluid density, $\vec{u}$ fluid velocity vector, S_m source term for mass within the fluid.
The first term on the left side describes how the mass of the fluid changes over time. The second term on the left side shows how the mass flow of the fluid phase diverges at a given point calculated by the divergence operation.

- The conservation of momentum describes the balance between the forces acting on the fluid particles and the resulting acceleration. For a Newtonian fluid, the momentum equations evolve into the Navier-Stokes equations that governs the motion of fluid elements, considering the effects of pressure forces, viscous forces, and gravitational forces (Ansys, 2021):

$$\frac{\partial}{\partial t}(\rho \vec{u}) + \nabla \cdot (\rho \vec{u}\vec{u}) = -\nabla p + \nabla \cdot (\bar{\bar{\tau}}) + \rho \vec{g} + \vec{F} \tag{2}$$

where p pressure, $\bar{\bar{\tau}}$ stress tensor, $\rho \vec{g}$ gravitational force, $\vec{F}$ external body force. However, in this work the external force is not considered.

The stress tensor can be calculated as given below (from the definition of a Newtonian fluid):

$$\bar{\bar{\tau}} = \mu \left[(\nabla \vec{u} + \nabla \vec{u}^T) - \frac{2}{3} \nabla \cdot \vec{u} I \right] \tag{3}$$

where μ molecular viscosity, I unit tensor.

- The energy equation is given below (Ansys, 2021):

$$\frac{\partial}{\partial t}(\rho E) + \nabla \cdot \left(\vec{u}(\rho E + p) \right) = \nabla \cdot \left(k_{eff} \nabla T - \sum_q \sum_j h_{j,q} \vec{J}_{j,q} + \left(\bar{\bar{\tau}}_{eff} \cdot \vec{u} \right) \right) + S_h \tag{4}$$

where k_{eff} effective thermal conductivity ($k + k_t$, where k_t is the turbulent thermal conductivity, $\vec{J}_j$ diffusion flux of species, $h_{j,q}$ specific enthalpy of species, S_h volumetric heat source.
The transport equations are described in section 4.2

4.2 Multiphase Flow Model

The simulation and analysis of fluid flows including various immiscible phases, such as liquids, gases, and/or solids, inside a single computational domain is referred to as multiphase flow. In multiphase flow, there are three methods as Eulerian Model, the Mixture Model and the Volume of Fluid (VOF) model. For this simulation, the VOF model was chosen because, when there are distinct boundaries or interfaces between several fluids in multiphase flows, VOF is especially well suited for simulating those flows. It is a reliable option for situations like free-surface flows (such as waves, sloshing liquids, and fluid-structure interactions) and phase-change because it can precisely represent the movement and interaction of these interfaces (Wu, 2022).

The Volume of Fluid (VOF) model in the ANSYS Fluent code is a widely used approach for simulating multiphase flows involving gas-liquid or liquid-liquid interactions and it is a simplified version of full Eulerian model for continuous-continuous phase interaction (Ansys, 2021). As noted above, the phase separation, free surface flows, and interfacial dynamics can all be simulated using the VOF model, which keeps track of the volume fraction of each phase within the computational cells. It makes possible to see and predict different multiphase flow patterns, like how bubbles, droplets, or liquid film waves behave in a fluid. The volume fraction of phase q is defined as the ratio of the volume of phase V_q to the total volume of the system V (Che, 2020):

$$\alpha_q = \frac{V_q}{V} \tag{5}$$

Immiscible phases are treated as a mixture in the VOF model, which uses a single set of momentum equations to simulate multiphase flow. The density and dynamic viscosity of the mixture are calculated by combining the parameters of each phase based on their volume fraction as shown below (Che, 2020):

$$\rho_m = \sum_q \rho_q \alpha_q \tag{6}$$

$$\mu_m = \sum_q \mu_q \alpha_q \tag{7}$$

For the resolution of the interface movement the volume fraction transport equation is utilized and written as follows (Cifani, 2016):

$$\frac{\partial \alpha}{\partial t} + \vec{u} \cdot \nabla \alpha = 0 \tag{8}$$

where u is the velocity of the mixture, t is the time.

In the VOF model, the energy E is given as a mass-averaged property:

$$E = \frac{\sum_{q=1}^{n} \alpha_q \rho_q E_q}{\sum_{q=1}^{n} \alpha_q \rho_q} \tag{9}$$

where E_q is calculated as shown below:

$$E_q = h_q - \frac{p}{\rho_q} + \frac{u^2}{2} \tag{10}$$

where h_q enthalpy. This variable depends on the change of shared temperature and specific heat of the phases.

4.3 Turbulence models

Turbulence modelling is a crucial in Computational Fluid Dynamics for simulating complex fluid flows, characterized by chaotic and irregular motion. Solving analytically the nature of turbulence is challenging since it is described by the nonlinear Navier-Stokes equation, which in two-phase flow originates also from the existence of multiple, deformable and moving interfaces and attendant significant discontinuities of fluid properties and complicated flow field near the interface. Therefore, an approximation of the physical behavior of turbulent flow is necessary to develop a mathematical model (Wilcox, 2006).

Based on calculated Reynolds number the flow was identified as turbulent (at Re>4000, the flow is allegedly turbulent in case of pipe). As stated before, modelling is necessary to solve three-dimensional turbulence effects. In CFD simulations, the eddy viscosity (or turbulence viscosity) term is introduced to account for the effects of turbulence, that occurs in fluid motion when there are rapid fluctuations in velocity and pressure at small scales. Instead of

resolving small-scale motions directly, which would be computationally expensive and infeasible for many practical cases, turbulence modelling techniques are employed to capture the impact of turbulence on the larger flow scales. The eddy viscosity concept is one such turbulence modelling approach. It assumes that the turbulent motion can be modelled as an additional "eddy" viscosity, which is added to the molecular (or laminar) viscosity of the fluid. This eddy viscosity is based on the idea that the small-scale turbulent eddies contribute to an effective viscosity, which varies with the local flow conditions and helps to account for the mixing and momentum exchange between the different fluid layers (Sadrehaghighi, 2018).

The most commonly used turbulence model that utilizes the eddy viscosity concept is the Reynolds-Averaged Navier-Stokes (RANS) model (Gorman, 2021). RANS equations provide a time-averaged representation of the turbulent flow that makes it easier to solve computationally. For example, the velocity and pressure can be decomposed into a mean value and a fluctuation value as shown below:

$$u_i = \overline{u_\iota} + u_i' \qquad p_i = \overline{p_\iota} + p_i' \tag{11}$$

where u_i and p_i instantaneous velocity in x direction and pressure, $\overline{u_\iota}$ and $\overline{p_\iota}$ mean velocity in x direction and pressure, u_i' and p_i' fluctuating velocity in x direction and pressure.
By doing so time averaged continuity and Navier-Stokes equations can be expressed as follows for incompressible flow (Wilcox, 2006):

$$\frac{\partial \overline{u_\iota}}{\partial x_i} = 0 \tag{12}$$

$$\rho \frac{\partial \overline{u_\iota}\,\overline{u_j}}{\partial x_j} = -\frac{\partial \bar{p}}{\partial x_i} + \frac{\partial}{\partial x_j}\left(\mu \frac{\partial \overline{u_\iota}}{\partial x_j} - \rho \overline{u_\iota' u_j'}\right) \tag{13}$$

where ρ fluid density, $\overline{u_\iota}$ and $\overline{u_j}$ Reynolds-averaged velocity components in the i and j directions, $\bar{p}$ Reynolds-averaged pressure, x_i, x_j spatial coordinates in the i and j directions, μ dynamic viscosity of the fluid, $\overline{u_\iota' u_j'}$ Reynolds stress tenso

4.3.1 The $k-\varepsilon$ model

There are several turbulence models based on RANS equations such as $k-\varepsilon, k-\omega$ SST Model (Shear Stress Transport Model), Spalart-Allmaras model etc.

Ren Y. et al. investigated the heat transfer during saturated boiling on the pool side of a spiral wound heat exchanger. They utilized the RNG $k-\varepsilon$ turbulence model and compared their findings with experimental data to understand the heat transfer characteristics in liquefied natural gas (LNG) applications. The results revealed a 13% deviation between the simulation and experimental outcomes (Yan, 2018).

Utilizing the $k-\varepsilon$ turbulence model, researchers carried out extensive studies on the flow and heat transfer properties within helically coiled tubes. Wu J et al. used the Realizable $k-\varepsilon$ model to study helically coiled tube-type heat exchangers with different tube diameters (12, 19, 25 mm), tube pitches (50, 100, 150 mm), and helical radii (100, 150, 200 mm). They examined gas-liquid distribution, vapor volume fractions, heat transfer coefficients, and pressure drops. Results showed that, during boiling, liquid collected at the tube's bottom, mixing with gas, while gas concentrated near the inner side and upper part of the coil (Wu, 2022).

The $k-\varepsilon$ model is used in this work because of its computational efficiency, applicability for complex geometries like helical coil. Therefore, brief information about this model is provided below.

As mentioned in section 4.3 the $k-\varepsilon$ model is a two-equation model and uses RANS equation for solving the complete flow field. In this model, there are two transport equations (for k and for ε) that need to be solved (Wilcox, 2006).

1. The turbulence kinetic energy (k) (Wilcox, 2006):

$$\frac{\partial k}{\partial t}+u_j\frac{\partial k}{\partial x_j}=\tau_{ij}\frac{\partial u_i}{\partial x_j}-\varepsilon+\frac{\partial}{\partial x_j}\left[(\nu+\nu_T/\sigma_k)\frac{\partial k}{\partial x_j}\right] \tag{14}$$

where k turbulence kinetic energy, τ_{ij} Reynolds stress tensor, ε turbulence dissipation rate, ν kinematic viscosity of the fluid, ν_T turbulent viscosity (eddy viscosity), σ_k turbulent Prandtl number for turbulence kinetic energy (constant).

Equation (14) is a measure of the energy associated with turbulent fluctuations. The equation for k is derived from the transport equation for the Reynolds stress and includes terms for turbulent kinetic energy production, dissipation, and diffusion.

2. The dissipation rate (ε)

$$\frac{\partial \varepsilon}{\partial t} + u_j \frac{\partial \varepsilon}{\partial x_j} = C_{\varepsilon 1} \frac{\varepsilon}{k} \tau_{ij} \frac{\partial u_i}{\partial x_j} - C_{\varepsilon 2} \frac{\varepsilon^2}{k} + \frac{\partial}{\partial x_j} \left[(\nu + \nu_T / \sigma_\varepsilon) \frac{\partial k}{\partial x_j} \right] \tag{15}$$

Where $C_{\varepsilon 1}, C_{\varepsilon 2}$ empirical constants (=1.44 and 1.68, respectively), σ_ε turbulent Prandtl number for turbulence dissipation rate (constant=0.72).

As mentioned earlier, a two-equation model belongs to the eddy viscosity models category, which involve the derivation of two transport equations. So, in the eddy viscosity models the Boussinesq assumption is a simplification used to model the Reynolds stresses in the time-averaged Navier-Stokes equations and it is given below (Davidson, 2022).

$$\tau_{ij} = -\overline{u_i' u_j'} = 2\nu_T S_{ij} - \frac{2}{3} k \delta_{ij} \tag{16}$$

where u_i', u_j' velocity fluctuation component in i and j direction, respectively, δ_{ij} Kronecker delta function, S_{ij} main strain-rate tensor.

The Kronecker delta is a mathematical expression for linear algebra and it is defined as follows:

$$\delta_{ij} = \begin{cases} 1, & i = j \\ 0, & i \neq j \end{cases} \tag{17}$$

The turbulent viscosity ν_T is defined for $k - \varepsilon$ model as presented below:

$$\nu_T = C_\mu \frac{k^2}{\varepsilon} \tag{18}$$

where C_μ model coefficient (=0.09).

4.4 Evaporation-Condensation Model

There are several developed phase change models such as Lee model, temperature recovery model, phase field model, heat flux balance model, and empirical correlation model (Liu, 2020). The Lee model is frequently used in various research studies as evidenced by its application on subcooled water jet impingement cooling on superheated surfaces (Moon, 2022) and a 2D hydrofoil moving in two-layer stratified fluid (Kim, 2021). In the ANSYS Fluent code, the Lee model is only available option for interphase mass transfer through condensation-evaporation when using the Volume of Fluid (VOF) model.

The Lee model calculates the vapor transport equation governing the liquid-vapor mass transfer as follows (Ansys, 2021):

$$\frac{\partial}{\partial t}(\alpha_v \rho_v) + \nabla \cdot \left(\alpha_v \rho_v \vec{U}_v\right) = \dot{m}_{lv} - \dot{m}_{vl} \tag{19}$$

where v vapor phase, α_v vapor volume fraction, ρ_v vapor density, $\vec{U}_v$ vapor phase velocity, $\dot{m}_{lv},\ \dot{m}_{vl}$ rates of mass transfer due to evaporation and condensation.

5 Methodology

This section provides a setup with boundary conditions used in the simulation. It should be noted that only single helical coil was considered, and not four as in the MOTEL facility. Thus, the developed model was used to show the principles of the simulations. However, for a more realistic modelling, all the coils should be considered.

In this work there are two cases referred as case-1 and case-2.

- *Case-1*. A separated single helical coil steam generator simulation with prescribed boundary conditions at the tube walls. Case-1 was modelled to dissociate the simulation of boiling in the tube from the heat transfer from the pool to the tube, so that it is verified, that the boiling is modelled properly, and that the sensible results with both boiling in the tube and heat transfer from the pool are not due to eventual compensating errors. This study considers the appropriate boundary conditions and basic assumptions focusing on a single helical coil steam generator setup. The constant temperature assumption is one of the main assumptions used in this investigation. This presumption is specifically based on the primary side of the facility's operating pressure, which is limited to a maximum of 4 MPa.

- *Case-2*. The single helical coil steam generator immersed in a cylindrical pool. In this scenario, two boundary conditions are applied for the simulation, corresponding to both the primary and secondary sides of the MOTEL facility. To accommodate these conditions, a User Defined Function (UDF) was developed in C++ programming language.

Each subsection provides details regarding the development of geometries, mesh generation, physical modelling, and boundary conditions applied in the simulation. It also includes discussions on numerical grid independence for single helical coil steam generator and convergence study for both geometries to ensure validation of the results.

5.1 Development of the single helical coil steam generator geometry (case-1)

A detailed 3D model of the helical coil steam generator was created using build-in tool in ANSYS 2021 R2 called DesignModeler. There are three different plugins in ANSYS for creation of the geometry: SpaceClaim, Discovery and DesignModeler. Among these options, DesignModeler has specific advantages for complex geometries such as helical coil. It has significant capabilities for modifying geometric shapes utilizing parameters and measurements.

Using features in DesignModeler, two distinct regions (fluid and solid) were generated for the single helical tube. A cavity was employed to define the space between the inner tube and outer casing. Subsequently, a Boolean operation was applied to effectively partition these two regions, resulting in the precise definition of distinct fluid and solid regions within the tube.

Table 3 presents the dimensions utilized to model the helical coil steam generator in the simulation. The visualization of the created model of the SG is provided below in Figure 6:

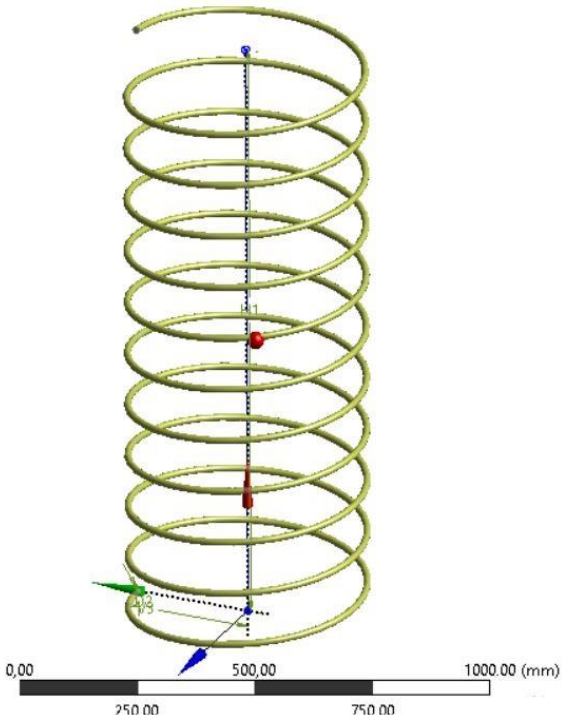

Figure 6. The geometry of the helical coil steam generator

5.2 The helical coil steam generator immersed in a cylindrical pool (case-2)

As described in subsection 5.1 the same method was used for the geometry creation and mesh generation with built-in DesignModeler tool and meshing tools within the ANSYS Fluent, respectively. However, in this case outer pool is added to the single helical coil tube, which requires defining the solid and fluid regions with additional inlet and outlet on the pool for the fluid coming from the core at a certain temperature and pressure. By this model the conjugate heat transfer is solved, which means that conduction and convection heat transfer phenomena is accounted. The created geometry is shown in Figure 7.

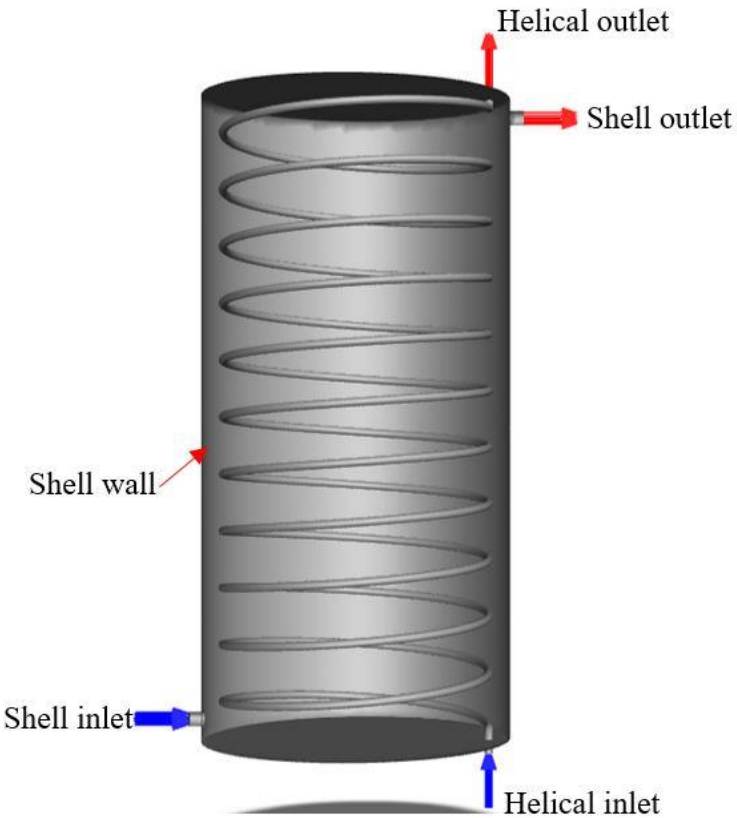

Figure 7. The helical coil steam generator in a cylinder

The mesh shown in Figure 8 was generated by importing the created geometry into the Mesh module. The helical part was meshed using sweep mesh settings to capture its structure, while the pool part was meshed using a sizing method to adapt to its complexity. The helical coil part of the mesh is structured hexahedral, as seen in Figure *8*b, while the pool part is tetrahedral as seen in Figure *8*a. In the Mesh module, specific components of the geometry were labelled with appropriate names. In order to ensure accurate simulation, specific

components of the geometry were labelled with appropriate names using distinct faces. The number of elements summary generated is shown in Table 4.

Table 4: Pool and helical coil mesh description

Mesh	Total number of elements	Number of elements in helical fluid region	Number of elements in helical solid region	Number of elements in pool fluid region
1	5 364 704	716 037	637 749	4 010 918

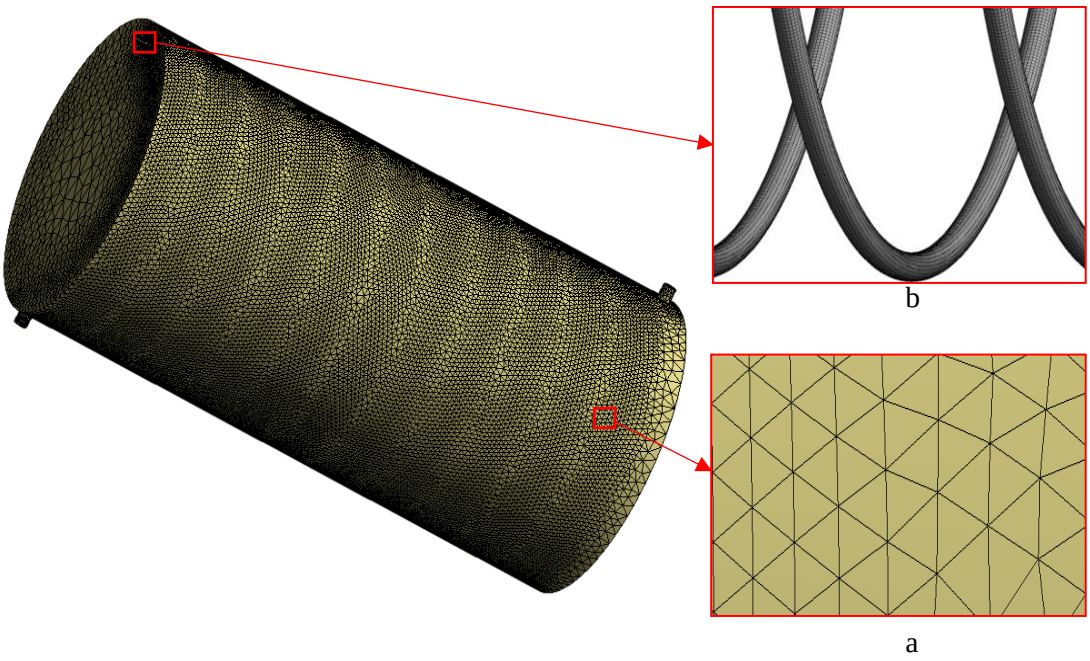

Figure 8. Generated mesh for the pool and helical coil tube

5.3 General setup for both cases

After exporting meshed geometry to the pre-solver to set up the simulation the following conditions was chosen to accurately model the behavior of the helical coil steam generator. The first step was defining phases within the ANSYS Fluent. In the Multiphase model, the VOF model with implicit model and with implicit body force has been selected considering the complex nature of the system and the presence of the multiple phases. As explained in section 4.2 the pressure-based VOF model is known for its effective capturing of phase change phenomenon in general. In particular, the VOF model with an implicit body force

was considered due to its efficient simulation of sharp phase interfaces and complex flow patterns. After selecting all properties in the VOF model, the energy was turned on since heat transfer is supposed to occur. For turbulence modelling, as discussed earlier, the $k-\varepsilon$ model with enhanced wall treatment was chosen. In the $k-\varepsilon$ turbulence model, the Standard Wall Function is chosen for higher accuracy and stability near solid walls, considering the dimensions of the helical coil steam generator of the MOTEL facility (because in scenarios with thin boundary layers or adverse pressure gradients this treatment captures near-wall physics). Figure 9 illustrates major steps chosen models used in the simulation.

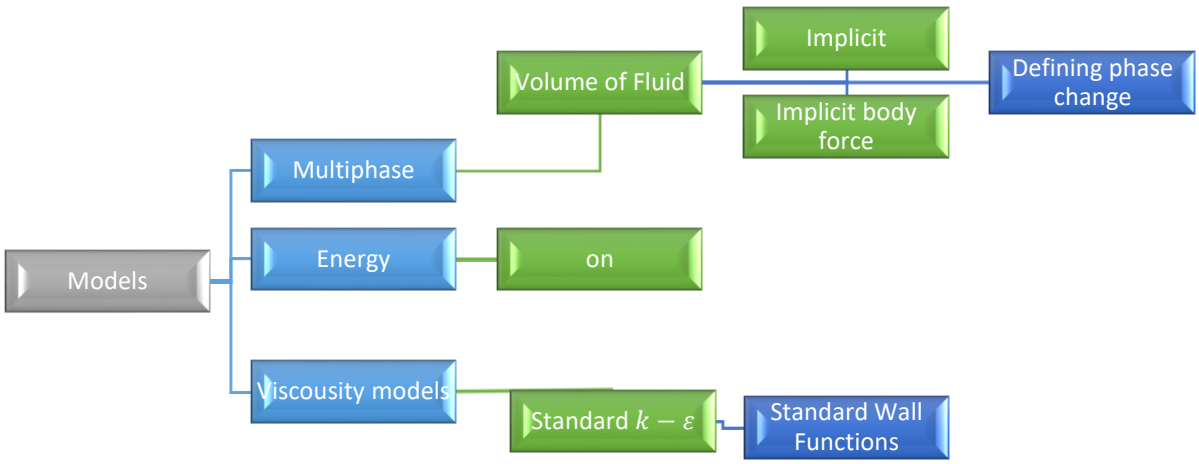

Figure 9. Flow chart of preprocessing

The next step involved selecting materials from the Fluent database. Liquid water and water-vapor were chosen for the fluid phase, while steel properties were copied to the material library for the solid phase.

5.3.1 Simulation setup for case-1 with boundary conditions

The overall setup for this case aligns with what was previously mentioned, with one notable exception. Specifically, the phase change model chosen for the separated single helical coil steam generator is the evaporation-condensation model, selected for its precision in

simulating the boiling phenomenon inside the tube. The boundary conditions for the simulation are given in Table 5.

Table 5: The used boundary conditions for single helical coil.

Parameters	Inlet	Outlet	Wall
Velocity [m/s]	4	-	-
Pressure [MPa]	0.5	0.5	-
Temperature [K]	416	-	473
Material	liquid water	-	steel
Slip condition	-	-	No slip

5.3.2 Simulation setup for case-2 with boundary conditions

In the second case, the general setup, as described in section 5.3 was used. However, the heat transfer process was executed using a user-defined function (UDF), which was written in C++ programming language. For crucial characteristics like saturation temperature and latent heat of vaporization, this UDF included macros. The main equation utilized in the code can be found in Appendix 1.

Materials, specifically liquid water, water-vapor and steel were selected from Fluent materials database. Nevertheless, to improve the accuracy of the simulation properties of water and vapor such as density, thermal conductivity, heat capacity, viscosity, enthalpy, and the speed of sound were dynamically adjusted using with UDF code. These property modifications were achieved by generating data in CoolProp library within Microsoft Excel and then integrating these custom property values into the ANSYS Fluent library. Using the tables for phase change simulations is important since the definition of enthalpies (and thus the latent heat) helps to obtain good results and/or smooth convergence.

This approach was adopted to ensure that simulation results close to real-world conditions, considering the variations in water and vapor properties with changes in pressure and temperature.

A parametric study was required due to the lack of values from the experiment. Therefore, to investigate the thermal and fluid dynamic behavior of a helical coil immersed in a

cylindrical enclosure two different temperatures, specifically 463 K and 473 K were simulated. The boundary conditions of the second case are summarized in Table 6.

Table 6: Boundary conditions for the case-2

Parameters	Primary side		Secondary side		Wall
	Inlet	Outlet	Inlet	Outlet	
Velocity [m/s]	1	-	4	-	-
Pressure [MPa]	2	2	0.5	0.5	-
Temperature [K]	463 / 473	-	416	-	coupled
Material	liquid water	liquid water	liquid water	water-vapor	steel
Slip condition	-	-	-	-	no slip

5.4 Mesh and convergence study for case-1

In CFD, the main objectives of the mesh independence study are to evaluate the impact of mesh resolution on numerical solution accuracy and convergence. In case of the helical coil steam generator, mesh quality is important for accurate predictions, especially near the coil surface and regions with heat transfer.

The Mesh module in the ANSYS Fluent was used to produce structured hexahedral meshes that matched the helical coil geometry. Additionally, the fluid inlet and outlet, as well as the helical wall was defined within the computational domain.

The mesh independence study was conducted for the single helical coil. For the computational domain, four mesh configurations were chosen as shown in Table 7. The mesh configurations differ in size, with cell counts of 299 376, 501 896, 983 336, and 1 085 858, respectively. Additionally, the number of elements in the fluid and solid regions varies between configurations.

Table 7: Single helical coil mesh comparison

Mesh	Total number of elements	Number of elements in fluid region	Number of elements in solid region
1	299 376	129 276	170 100
2	501 896	295 864	206 032
3	983 336	762 868	220 468
4	1 085 858	846 770	239 088

Table 8 presents a comparison of various properties, including temperature, liquid water volume fraction, velocity, density, and the y+ range. This comparison is conducted for different mesh configurations at a specific height (655.5 mm) within a helical coil. In this analysis, changes below a 5% threshold are considered acceptable. It is worth to note that:

- Changes in temperature are consistently small, remaining below 0.5% across all mesh configurations.

- On the other hand, other properties exhibit varying degrees of sensitivity to mesh changes:

Between Mesh 1 and Mesh 2, variations exceeding 7% are observed in the volume fraction of the fluid, velocity, and density. Comparing Mesh 3 to Mesh 4, differences are consistently below 5% for all properties, indicating improved convergence and mesh independence. The largest variation is seen in velocity, which is 4.51%.

- Regarding y+ values, it is observed that both Mesh 3 and Mesh 4 fall within the range of 42 to 171. This range aligns with the requirements for simulations using a log layer fitting function, confirming that these mesh configurations appropriately resolve the boundary layer for the specific simulation.

Table 8: Mesh independence study results

Mesh	T, [K]	δ_T, [%]	q_l	δ_q, [%]	u, [m/s]	δ_u, [%]	ρ [kg/m3]	δ_ρ, [%]	y+ range
1	469.11	-	0.281	-	15.3	-	285.7	-	110-776
2	467.00	0.450	0.302	7.47	13.3	13.01	306.7	7.35	114-229
3	467.61	0.131	0.289	4.31	11.1	16.54	290.0	5.43	42-171
4	467.79	0.038	0.278	3.81	10.6	4.51	287.5	0.86	55-111

Therefore, after conducting mesh independence study it was decided to select Mesh 3 for further investigations. Figure 10 shows generated mesh for the single helical coil.

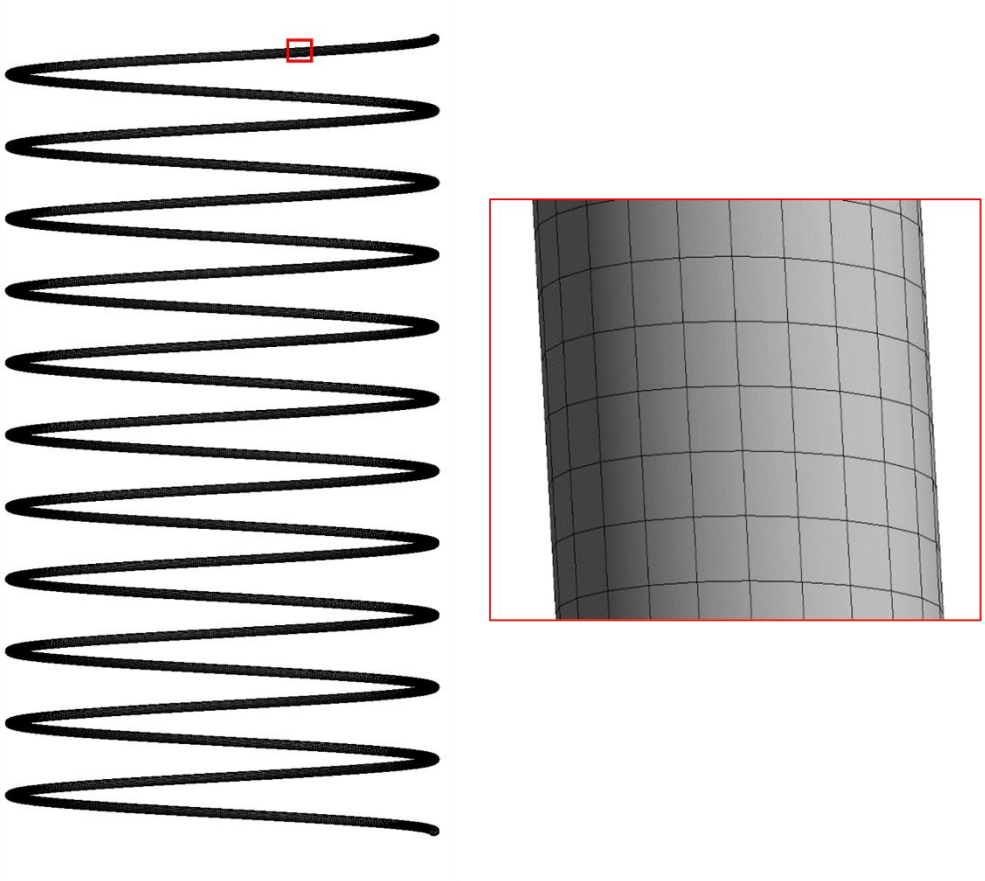

Figure 10. Single helical coil mesh

Convergence study using Mesh 3

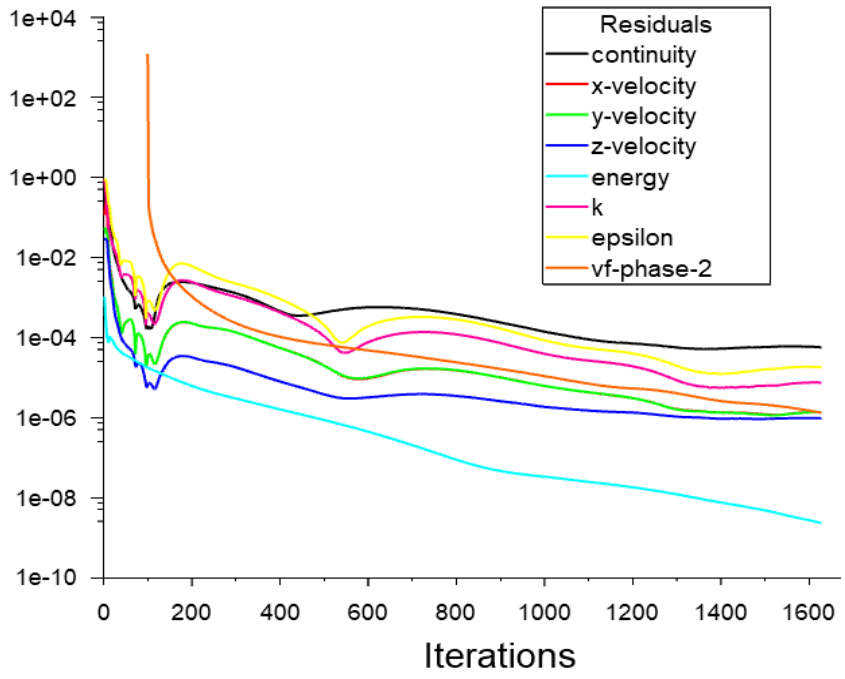

Figure 11. Convergence study

From Figure 11, it can be seen that the simulation has converged to a level below 10^{-3}. The convergence criteria were set to a minimum of 10^{-8}. All parameters reached convergence after 1400 iterations. The highest value is observed in the continuity equation, which is approximately 10^{-4}, while the lowest is in the energy equation, below 10^{-8}.

The figure depicts a sharp drop in the red line, representing 'vf-phase-2,' occurring around the 100th iteration. This drop corresponds to the phase change when the liquid temperature reaches the saturation temperature.

6 Results and discussion

This section contains an overview of the simulation results for a separated single helical coil and one immersed in a water pool, as mentioned in the methodology section.

6.1 Results of the simulation for case-1 (Mesh 3)

Figure 12 shows the temperature contour of the helical coil tube and cross-sectional views on the right side. It is visible that after three turns the saturation temperature is reached at the wall, which can be confirmed from Figure 13 as phase change started from that point. The mixture temperature reaches saturation at elevation 0.35 m. The temperature difference between the inlet and the outlet is 57 K and the volume fraction at the outlet is around 0.85. From cross-sectional views, it can be observed that the fluid temperature increase propagates from the coil wall towards the center of the tube. Near the outlet the fluid is in thermal equilibrium with the coil wall.

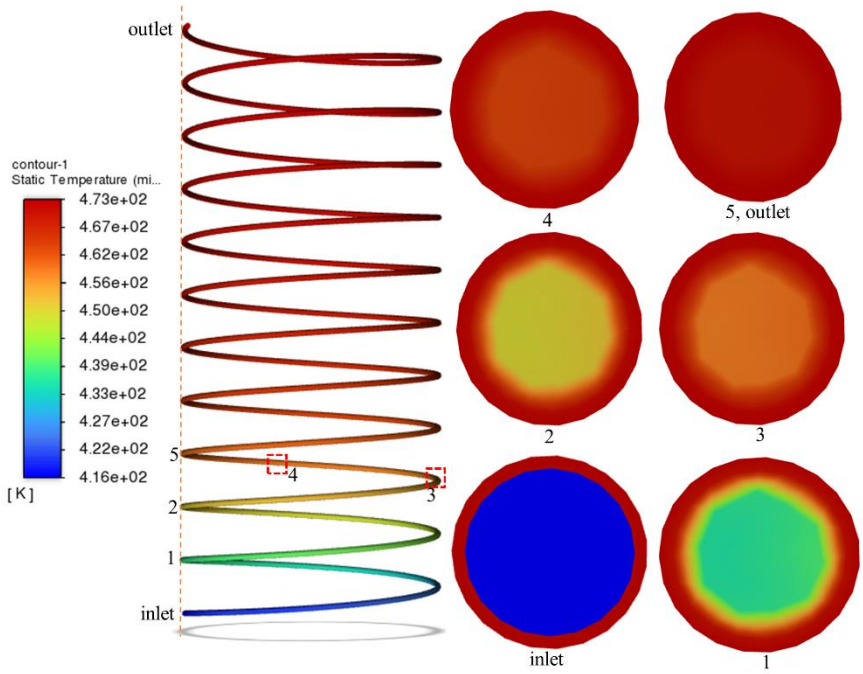

Figure 12. Temperature contour in helical coil tube (case-1)

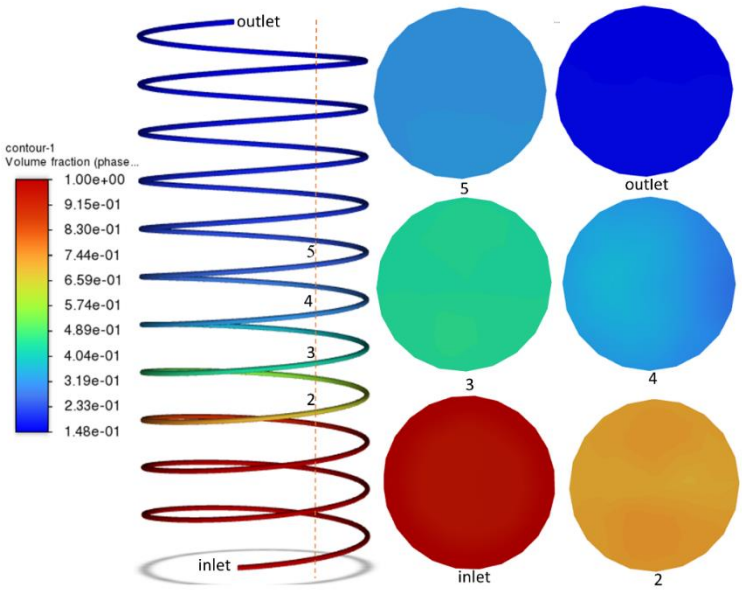

Figure 13. Volume fraction of liquid water in helical coil tube (case-1)

The decrease in the volume fraction of liquid water in the coil is displayed in Figure 13. The liquid water volume fraction initially has a maximum value of 1, indicating that the fluid is entirely liquid. However, as the fluid moves through the coil, the liquid water volume fraction decreases significantly, eventually reaching a low value of 0.148 as it exits the coil at the outlet. A point labelled as "2" in the figure marks the starting turn of this phase transition phenomenon. When a fluid reaches its saturation temperature, it begins a shift from a single-phase (pure liquid) to a two-phase (liquid-vapor) condition. This change is visually represented on the right side of the figure, where cross-sectional views are provided, corresponding to specific points of interest.

Figure 14 furthers this understanding by displaying the fluid density distribution across the helical coil. When the liquid water volume fraction is high (near 1), the fluid has a density of around 998 kg/m^3. However, when the fluid moves towards the coil's outlet, it undergoes phase change and thermal expansion, resulting in a significant shift in density. By the time the fluid reaches the outlet, the density of the liquid-gas mixture has dropped to around 100 kg/m^3. This drop in density can be traced to the change from a primarily liquid phase to a two-phase condition, with the vapor phase contributing to the total density decrease.

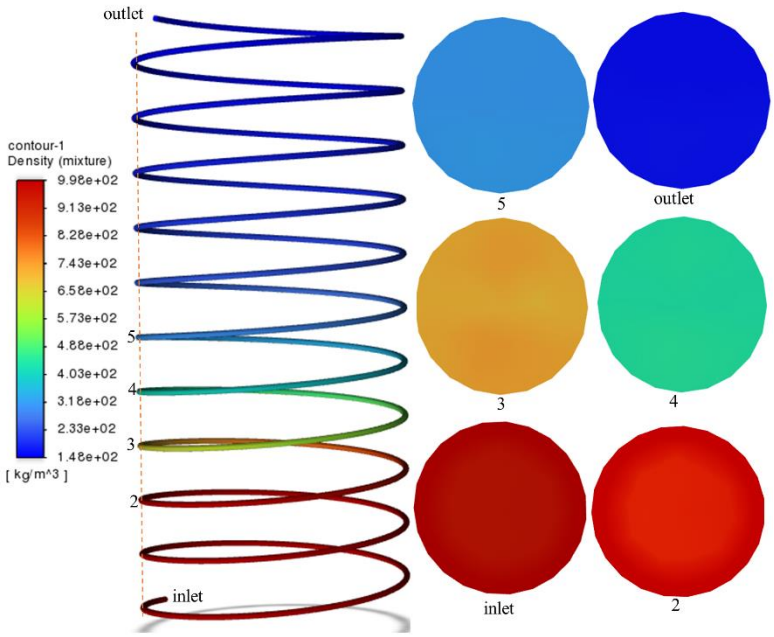

Figure 14. Density distribution of liquid-gas mixture in helical coil tube (case-1)

Figure 15 illustrates the velocity profile. It is observed that initially the velocity was around 4 m/s, and it started to increase after the beginning of phase change. This rise in velocity is closely related to the decrease in liquid phase density, which is a direct result of the phase transition and thermal expansion processes. The presence of the vapor phase, which is naturally less dense than the liquid phase, can explain this increase in fluid velocity. As a result, the vapor phase helps to reduce overall fluid density, allowing for faster fluid motion. The highest velocity was obtained around 30 m/s when the vapor occupied 85.2 % of the volume.

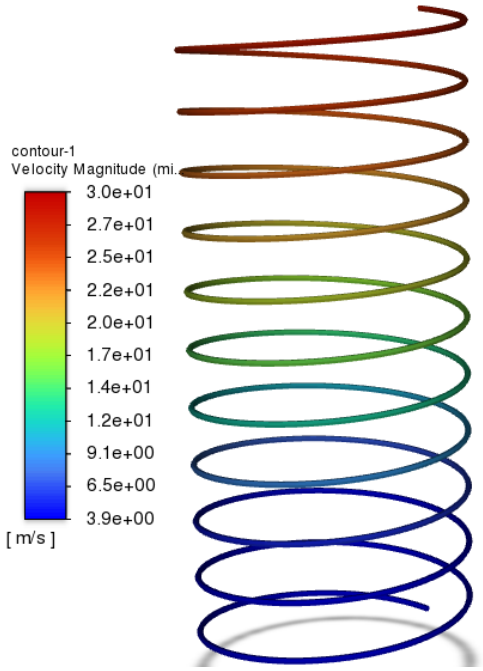

Figure 15. Velocity profile in helical coil tube (case-1)

6.1.1 Analysis of the results for case-1

The axial temperature profile is plotted in Figure 16. The taken points are shown in Figure 12 with labelled numbers. The temperature is increasing with height and the increment is steeper near the helical coil inlet. Once the temperature reaches the saturation point, it remains constant. This is because the energy added is used for phase change (latent heat) rather than raising the temperature (sensible heat). The temperatures at the helical coil's inlet and outlet are 416 K and 473 K, respectively. Notably, the outlet temperature matches the saturation temperature, which occurs at approximately 0.35 m height.

Figure 17 displays the axial mixture density profile. The density is the highest at the helical coil inlet and the fluid is only liquid water. The density decreases while moving upwards in the coil. This is due to thermal expansion of the fluid below the saturation point (single-phase flow) and vapor formation beyond the saturation point (two phase flow). At the inlet, where the fluid is entirely in the liquid state, the density is 998 kg/m^3. However, at the outlet, where a mixture of liquid and vapor is present, the density decreases to 148 kg/m^3.

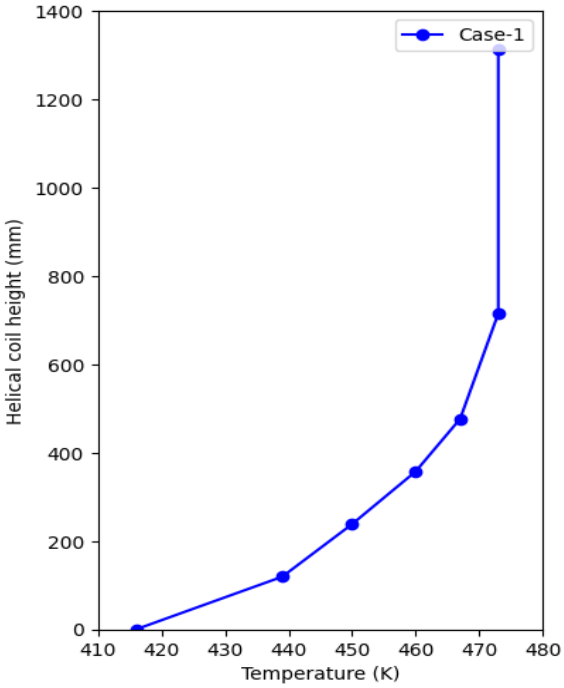

Figure 16. Axial temperature profile of the helical coil tube (case-1)

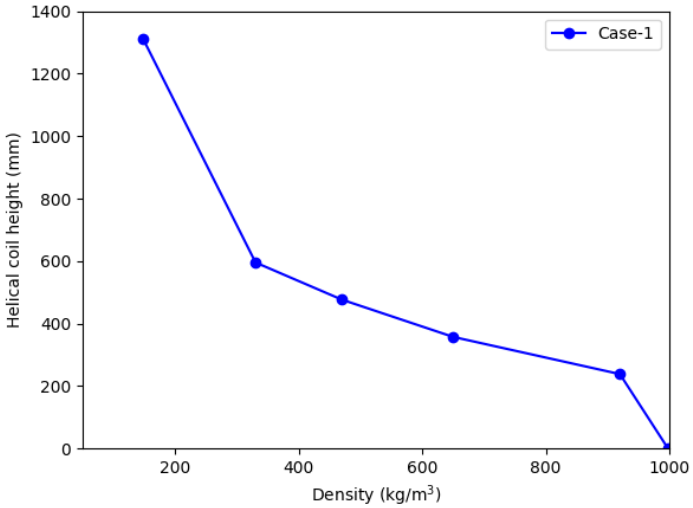

Figure 17. Axial density profile of the liquid-gas mixture (case-1)

Figure 18 shows the phase-1 axial volume fraction profile. At the inlet the volume fraction of the liquid water has a value of 1. It starts to decrease at the elevation of around 0.35 m when the fluid temperature exceeds the saturation temperature. At the outlet the volume fraction of water-vapor is around 85 %.

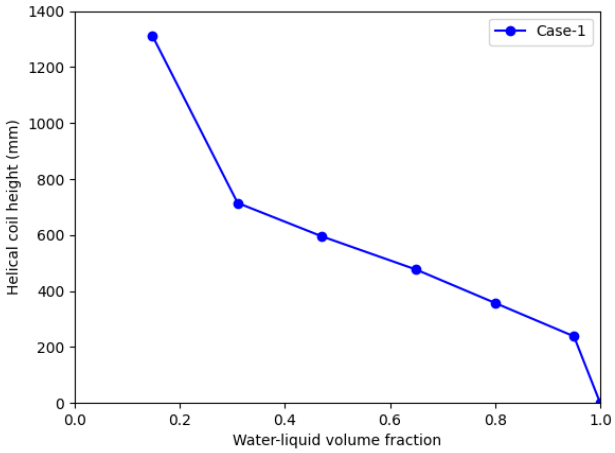

Figure 18. Axial volume fraction profile of the liquid water (case-1)

Figure 19 shows the axial velocity of the fluid. The velocity profile is analogous to the density profile. The mixture velocity increases while moving towards the outlet. This is to ensure conservation of the mass flow rate since the density is decreasing. At the inlet, the velocity is 3.9 m/s, while at the outlet, it reaches 30 m/s.

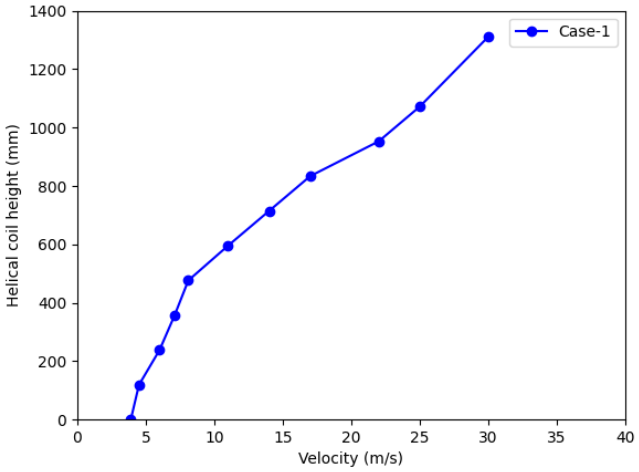

Figure 19. Axial velocity profile of the liquid-gas mixture (case-1)

6.2 Results of the simulation for case-2 at 463 K and 473 K pool inlet temperatures

6.2.1 Results at 463 K temperature

Figure 20 and Figure 21 show the temperature distribution of the single helical coil immersed in a cylinder, with a cross-sectional view presented on the right in Figure 21 at 463 K pool inlet temperature. These visual representations illustrate how the working fluid enters the steam generator helical coil tube at an initial temperature of 416 K and rises through the tubes. During this rise, heat is transferred from the primary side, resulting in a phase change on the secondary side. While exiting the system, the working fluid achieves a temperature of 463 K. This heat transfer mechanism happens due to convection, conduction, and radiation (but radiation is neglected for simplicity). The temperature difference between inlet and outlet of the coil is 47 K. The saturation temperature is reached around three and half turns which can be confirmed from Figure 22. After reaching the saturation temperature, the pool and the helical coil achieve a thermal equilibrium.

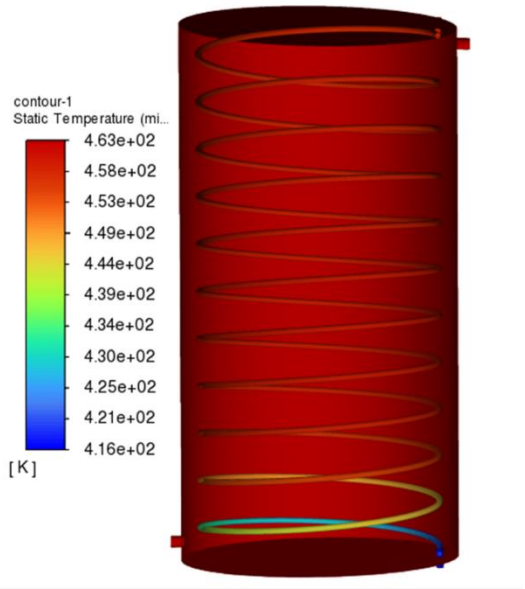

Figure 20. Temperature profile of the helical coil in a cylindrical pool at inlet temperature 463 K (case-2)

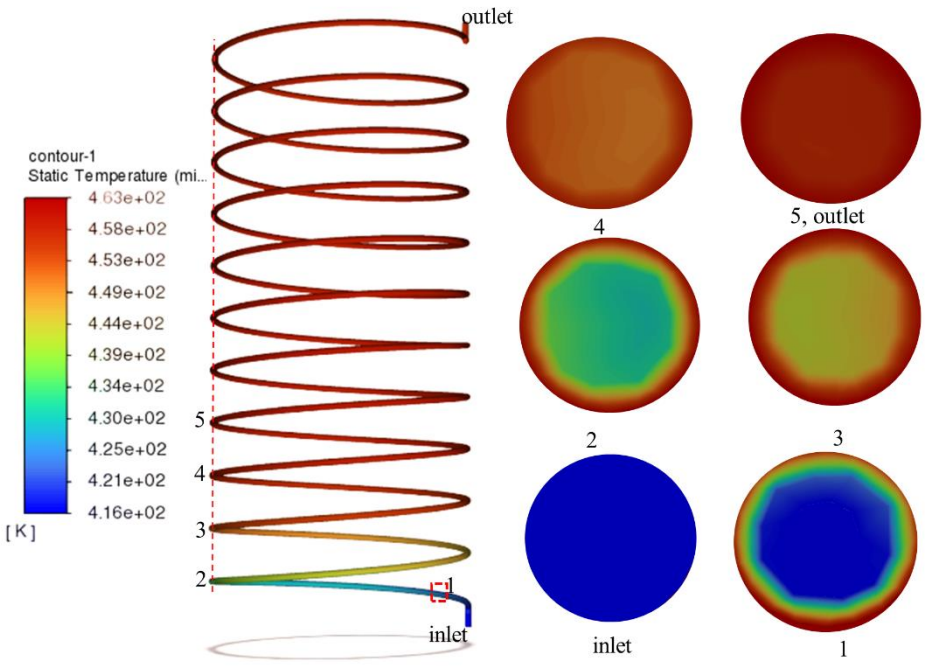

Figure 21. Distribution of temperature in helical tube at pool inlet temperature 463 K (case-2)

The cross-sectional view of the temperature profile shows the progression of heat from the helical coil's wall towards its center. The cross-section at the inlet shows a prevailing uniform temperature distribution, due to the inlet boundary condition. Moving through the cross-sectional views from “1” to “4”, it can be observed that temperatures are higher near the inner wall of the helical tube compared to the tube's center. This temperature gradient is a consequence of the heat transfer dynamics within the coil. Starting at point “5” and extending towards the outlet, the temperature profile becomes uniform. In this region, heat transfer processes have resulted in a more balanced temperature distribution.

Figure 22 illustrates the volume fraction of phase-1 at 463 K pool inlet temperature, representing liquid water phase. At the inlet, the mixture consists entirely of liquid water, indicated by a value of 1. As the fluid moves up within the helical coil, it heats up, eventually reaching the saturation temperature where boiling initiates. This phase change phenomenon is observed approximately after three and a half turns along the coil. The maximum volume fraction of phase-1, corresponding to water- liquid, is observed at the top of the helical tube, reaching a value of 0.209.

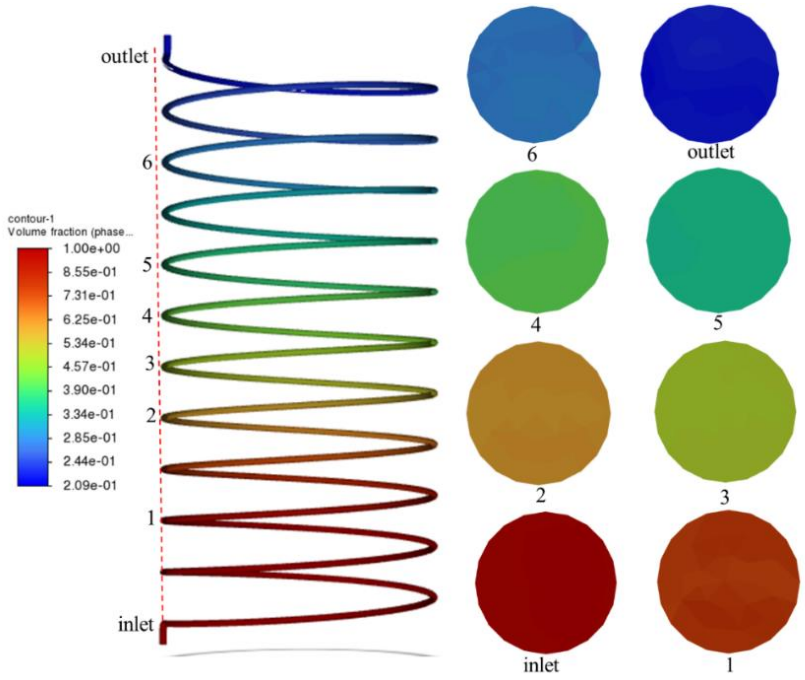

Figure 22. Volume fraction of the liquid water at pool inlet temperature 463 K (case-2)

Figure 23 shows the variation in density within the helical coil at 463 K pool inlet temperature. As previously stated, the starting point of the phase transition impacts the density of the mixture. The density enters at 998 kg/m^3 at the inlet of the coil, but as the fluid moves through the coil and the phase change begins, the density decreases. This drop is most noticeable at the exit, where the density is 187 kg/m^3.

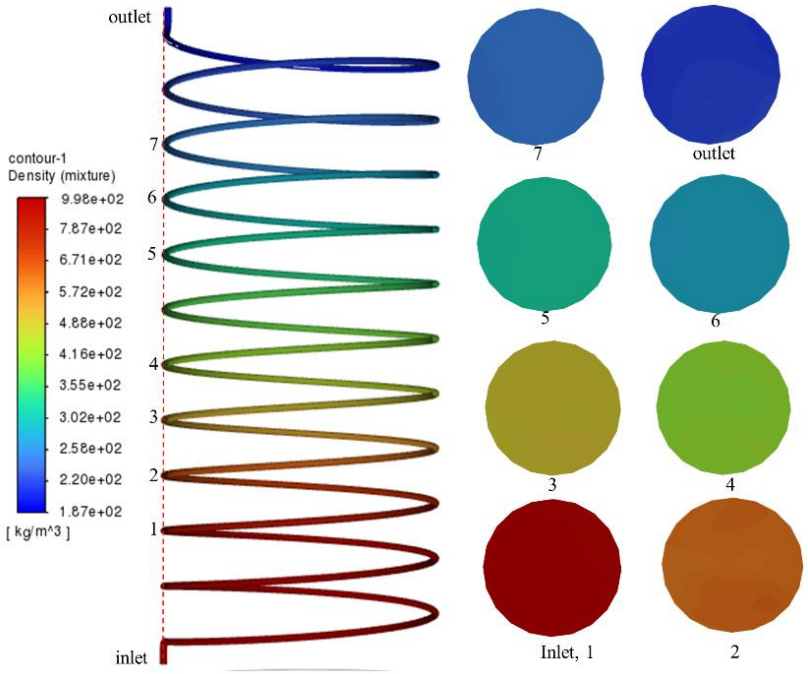

Figure 23. Density of liquid-gas mixture at pool inlet temperature 463 K (case-2)

Figure 24 shows the velocity profile of the working fluid at 463 K. The initial velocity within the coil was 2.77 m/s, but it increased after the phase change. The highest velocity is 34.7 m/s, and it occurs when the vapor occupies 80 % of the volume.

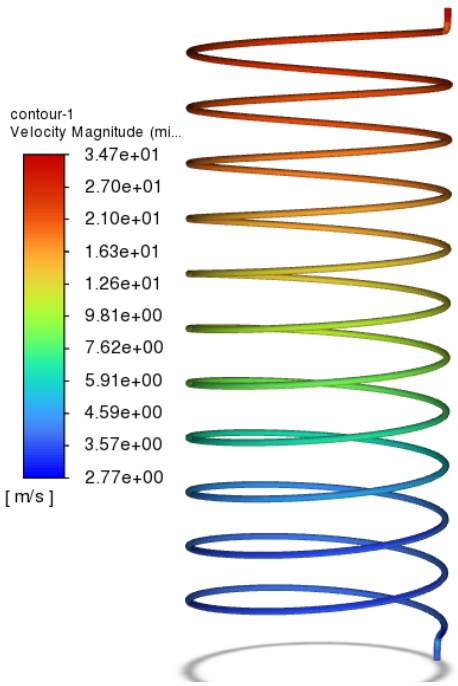

Figure 24. Velocity of liquid-gas mixture at pool inlet temperature 463 K (case-2)

6.2.2 Results at the 473 K pool inlet temperature

Figure 25 displays the temperature distribution within the helical tube at 473 K pool inlet temperature. The inlet temperature of the helical tube is 416 K, while the highest temperature, reaching 473 K, is observed at the top of the tube. This results in a temperature difference of 57 K between the outlet and inlet. As seen in Figure 26, the saturation temperature is reached at around 0.47 m of the helical coil height, corresponding to the beginning of the phase change.

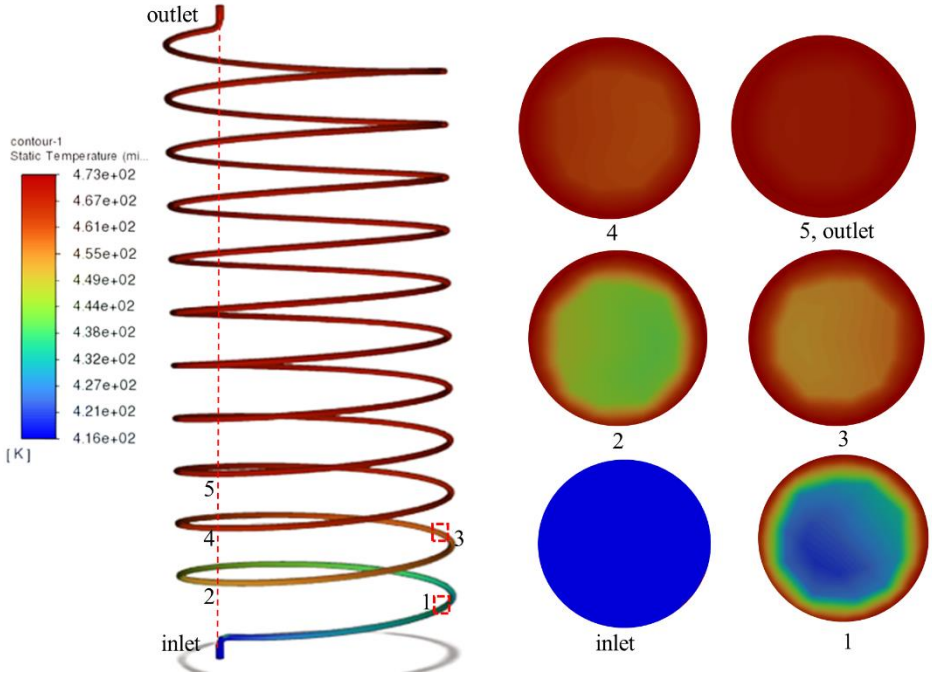

Figure 25. Temperature distribution in helical tube at pool inlet temperature 473 K (case-2)

Figure 26 displays the volume fraction of liquid water at 473 K pool inlet temperature. The volume fraction of the liquid water at the inlet and outlet is 1 and 0.173, respectively.

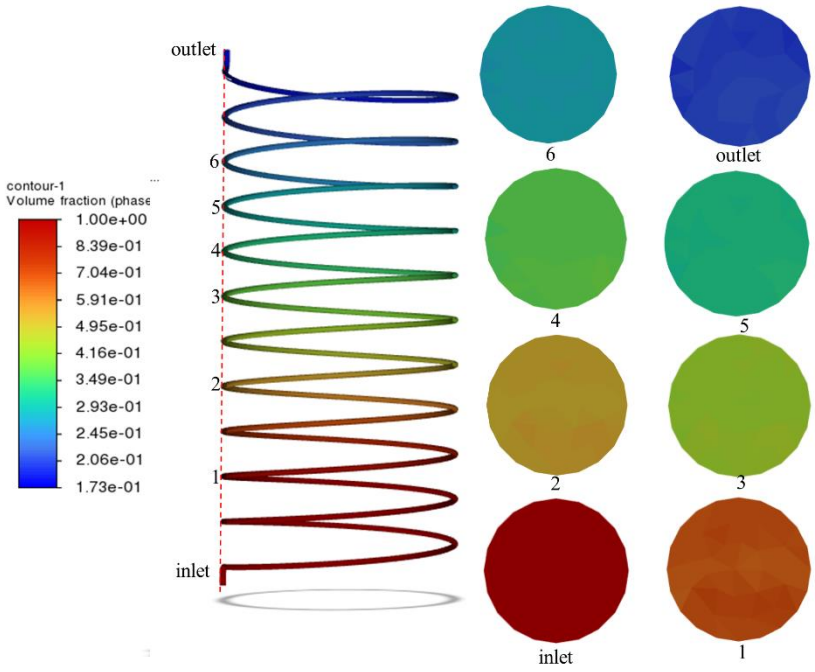

Figure 26. Volume fraction of the liquid water at pool inlet temperature 473 K (case-2)

Figure 27 shows the density of the working fluid for the case-2 at 473 K pool inlet temperature. The inlet density is 998 kg/m^3, while the outlet density is 157 kg/m^3.

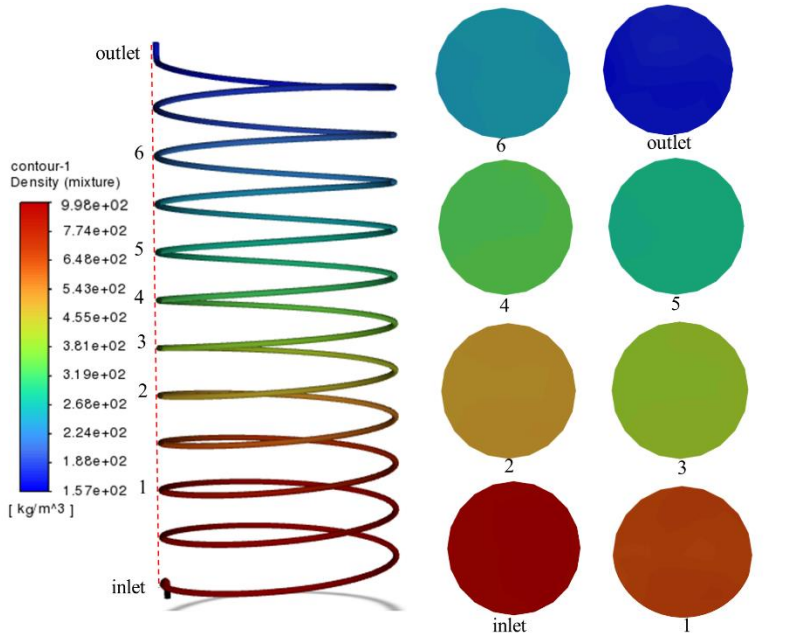

Figure 27. Density of liquid-gas mixture at pool inlet temperature 473 K (case-2)

The velocity distribution for the case-2 at 473 K inlet pool temperature is shown in Figure 28. As can be seen the inlet velocity of the fluid is 3 m/s, whereas the outlet velocity is 39.6 m/s.

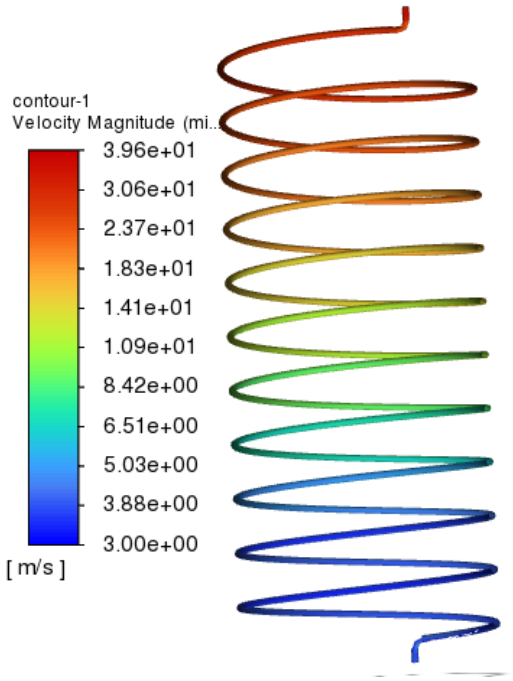

Figure 28. Velocity of liquid-gas mixture at pool inlet temperature 473 K (case-2)

6.2.3 Analysis of the results for case-2

Figure 29 shows the axial temperature distribution for 463 K and 473 K pool inlet temperatures. For both scenarios, the coolant temperature near the inlet is 416 K. The temperature difference between the 463 K and 473 K pool inlet scenarios increases with elevation. After saturation, the temperature difference between the coolant temperatures is 10 K.

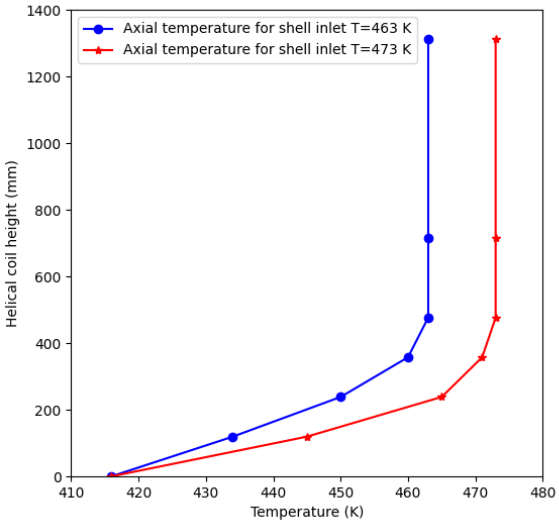

Figure 29. Axial temperature profiles of the helical coil for pool inlet temperatures 463 K and 473 K (case-2)

Figure 30 shows the volume fraction of the liquid water in terms of helical coil height. As can be seen, the results are qualitatively comparable, which supports the validity of the developed model. At the outlet the volume fractions reduce to 0.2 and 0.17 for pool inlet temperatures 463 K and 473 K, respectively. For both scenarios, a sharp drop of the volume fraction is observed from height of around 0.3 m to 0.65 m, because of the phase change.

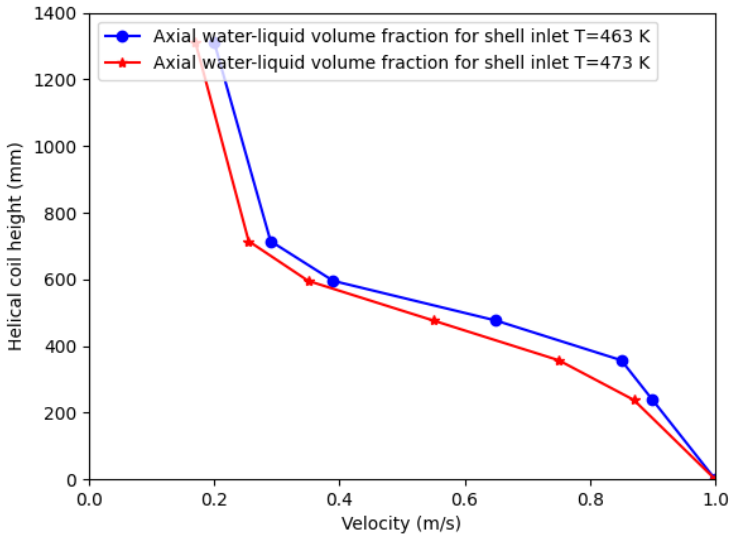

Figure 30. Axial volume fraction profiles of helical coil for pool inlet temperatures 463 K and 473 K (case-2)

Figure 31 illustrates the axial mixture density of the coolant for the 463 K and 473 K pool inlet temperatures. Initially, for both scenarios, the density was 998 kg/m³, and as elevation increases, it gradually decreases. The reduction in density near the helical coil inlet is relatively small. However, a more apparent reduction occurs at an elevation of around 0.47 m, corresponding to the starting point of boiling. As the volume fraction of vapor exceeds 0.5, the density change becomes less significant, indicating the conversion of most of the liquid water into steam.

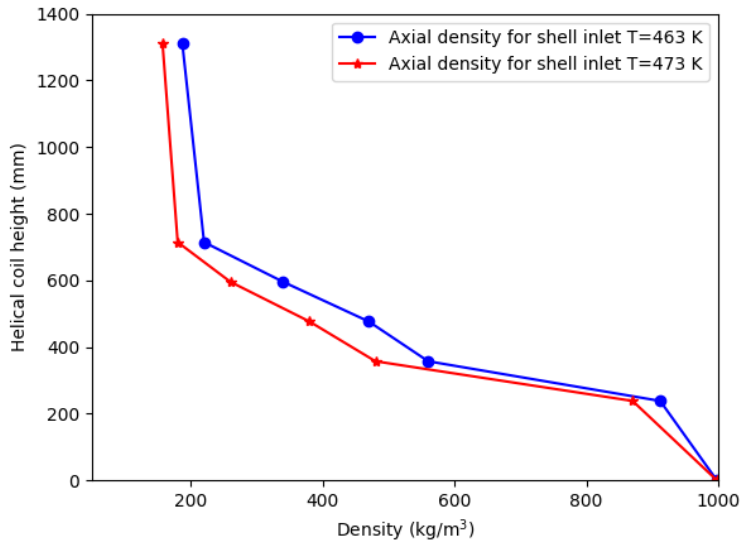

Figure 31. Axial density profiles of liquid-gas mixture for pool inlet temperatures 463 K and 473 K (case-2)

Figure 32 shows the axial mixture velocity profiles for pool inlet temperatures of 463 K and 473 K, with data points collected along each turn of the helical coil from inlet to outlet. For both temperature conditions, the velocity increases slowly with height near the inlet. As can be seen, the velocity is slightly higher at pool inlet temperature 473 K than at 463 K, demonstrating the impact of the higher temperature. At the outlet, the velocity in the 463 K scenario is 5 m/s lower than in the 473 K scenario, due to density difference.

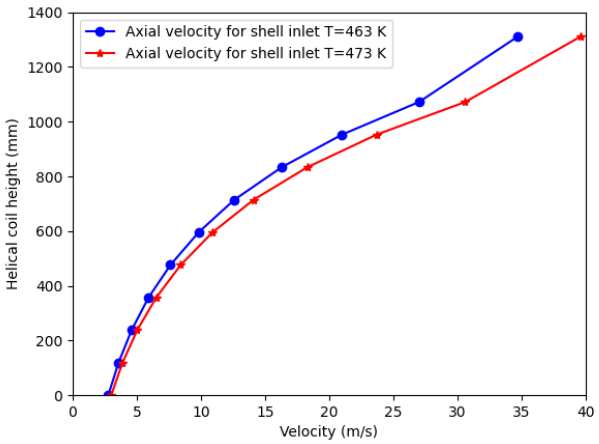

Figure 32. Axial velocity profiles of liquid-gas mixture (case-2)

Figure 33 compares the axial temperature profile of case-1 and case-2 with pool inlet temperature of 473 K. As can be noticed, the helical coil tube inlet temperature for both cases was initialized at 416 K. Overall the temperature profiles of the cases are in good agreement, however in case-1, the heat transfer is faster than in case-2. As a result, the temperature in case-1 reaches the saturation temperature at elevation of 0.35 m, whereas for the case-2 the saturation temperature is reached at a higher elevation (at 0.47 m). This discrepancy is because of the configuration of the system. In case-1 the heat transfer is between the helical wall and liquid inside the coil, therefore, is faster than case-2 (liquid inside the pool transfers the heat to the helical wall, then the heat is transferred to the helical fluid).

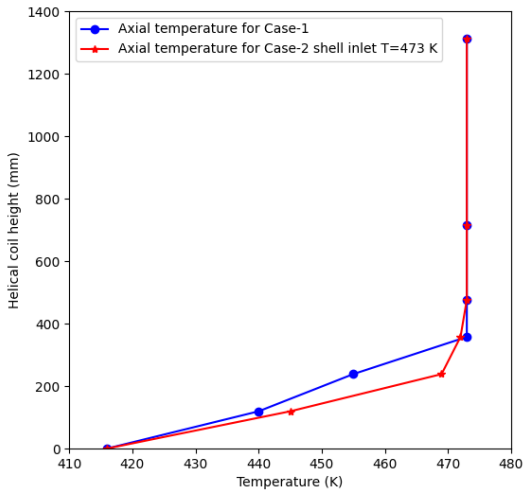

Figure 33. A comparison of the temperature profiles of case-1 and case-2 (pool inlet temperature 473 K)

7 Conclusion

The modular test facility MOTEL was built by LUT University in Lappeenranta in 2020 and was designed to resemble a pressurized water small modular reactor (SMR). Its main objective is to provide crucial information for code validation and provide insightful information about the operational dynamics of a prototype SMR working in a natural circulation environment.

The main objective of the thesis was to model part of the helical coil steam generator of the MOTEL test facility to obtain insights about phenomena that occur in the system. Therefore, a CFD analysis of part of the helical coil steam generator (that is, only a single coil was considered) was conducted. Additionally, CFD simulations provide some advantages over experimental work such as varying conditions that are uneasily achieved in experiments, and accessing areas that are physically difficult to investigate in experiments.

First, a literature review was carried out to gather information from existing experiments and simulations related to the helical coil steam generator. This helped to assign appropriate boundary conditions, as well as to select multiphase and turbulence models.

Two geometries (a separated single helical coil, referred as case-1, and a single helical coil immersed in a cylinder filled with water, referred as case-2) were developed using a built-in tool in the ANSYS Fluent code called DesignModeler. A mesh independence study was performed for the case-1 to determine a suitable cell size for higher accuracy. Using the FLUENT solver, the case-1 was investigated through the pressure-based volume-of-fluid (VOF) model and the $k-\varepsilon$ model. And the case-2 was investigated using a user-defined function (UDF) code written in C++ language instead of conventional Lee model for heat transfer modelling due to the pressure and saturation temperature difference between the primary and secondary side. Finally, the results were obtained and analysed. The major findings are:

- The temperature difference between the helical coil tube inlet and outlet was 57 K for case-1; for case-2, the two temperatures were 47 K and 57 K, because of two different temperatures prescribed at the pool inlet. For case-1, it was observed that around 0.35 m of the helical tube height, the saturation temperature was reached for

the mixture. For case-2, the saturation temperature for both scenarios was reached at around 0.47 m of the coil height.

- Density studies at the outlet and along the coil showed a significant drop in density for both cases, due to the boiling process. This decrease in density is important to understand the system's behavior and its consequences for phase transitions. The highest density occurred at the helical coil tube inlet (998 kg/m³) for all cases, where only liquid was present. Moving up, it dropped due to thermal expansion in the single-phase region below saturation. Beyond saturation, vapor formation further reduced it. At the outlet, with a liquid-gas mixture, the density for case-1 was 100 kg/m³, and for case-2 it was 187 kg/m^3 and 157 kg/m^3 for the pool inlet temperatures of 463 K and 473 K, respectively.

- The velocity in the helical coil tube was initialized at 4 m/s, but it quickly rose as the phase change continued and the density of the fluid mixture decreased. The highest observed velocity was about 40 m/s for case-2 with pool inlet temperature of 473 K, when a vapor volume fraction was 83 %, and 34.7 m/s was observed at 463 K temperature of the pool inlet. For case-1 the outlet velocity was 30 m/s.

- Lastly, case-1 and case-2 with pool inlet temperature of 473 K were compared. The results showed good agreement between them; however, in case-1, the saturation temperature was achieved at height around 0.35 m, while in case-2 it was achieved at height 0.47 m. The discrepancies in the height at which saturation temperature is reached in both cases might be due to variances in the boundary conditions used in the simulation. For case-1, a constant wall temperature boundary condition was used, where, the heat transfer was between the helical coil wall and fluid inside the coil. Whereas, for case-2, the heat transfer phenomena happened due to the inclusion of the primary side which means that liquid inside the pool transfers the heat to the helical wall, then the heat was transferred from the helical coil wall to the fluid inside the helical coil tube. These differences in boundary conditions influenced the thermal behavior of the helical coil. However, the temperature was increasing with the height for both cases till it reached the saturation point. After that it remained constant; nevertheless, the phase change was continued due to latent heat.

This work opens up some possibilities for future investigations. These are some examples:

- Due to the lack of main facility operating parameters, there were many trials to find appropriate boundary conditions for the simulation. It could be improved by having available operating values of pressure, temperature, and mass flow rate at various power ranges.

- Since the experimental results were not available during the preparation of the thesis, a validation of the CFD model was not fully completed. It could be solved after completing the scheduled experiments. A parametric study for different parameters i.e. heat flux and wall temperature, could be conducted in the future to ensure good agreement of the simulation with the experimental results.

- The effectiveness of the turbulence models such as SST $k-\omega$, Realizable $k-\varepsilon$, and RNG $k-\varepsilon$ etc. could be investigated by comparing simulations with the experimental results.

- The ANSYS Fluent code, like many computational fluid dynamics (CFD) software packages, offers various options for specifying material properties. These properties, such as density, viscosity, thermal conductivity, and specific heat, can impact the results of simulations. The choice of material property models, such as ideal gas, polynomial expressions, data from the US National Institute of Standards and Technology (NIST), or user-defined functions (UDFs), can affect both the accuracy and computational resources required for a simulation, and this issue could be further addressed.

- Uncertainty quantification could be investigated for material properties (density, thermal conductivity, and viscosity), inlet and outlet boundary conditions, and experimental results.

References

Alkan, C. 2022. Evaluation of safety transients in helical-coil steam generators with RELAP5-3D Code. University MASTER OF APPLIED SCIENCE (2022) Hamilton, Ontario (Engineering Physics).

Anderson, D., Tannehill, J. C., Pletcher, R. H., Munipalli, R., & Shankar, V. 2020. Computational Fluid Mechanics and Heat Transfer, CRC press.

ANSYS 2021. Ansys Fluent Theory Guide. 2600 ANSYS Drive, Canonsburg, PA 15317.

Che S. et al. 2020. CFD Simulation of Two-Phase Flows in Helical Coils. Frontiers in Energy Research, 8, 65, website: www.frontiersin.org.

Cifani, P, Michalek, W, Priems, G, Kuerten, J, Van Der Geld, C & Geurts, B. 2016. A comparison between the surface compression method and an interface reconstruction method for the VOF approach. Computers & Fluids, 136, 421-435.

Davidson, L. 2022. An Introduction to Turbulence Models. Department of Thermo and Fluid Dynamics. Chalmer University of Technology, Publication, 97(2), 1-8.

Gorman J. et al. 2021. Turbulence Models Commonly Used in CFD. Applications of Computational Fluid Dynamics Simulation and Modeling. IntechOpen.

Huang, J., Gou, J., Mao, H., & Shan, J. 2020. Development of a thermal-hydraulic analysis code for helically coiled once-through steam generator. Nuclear Engineering and Design, 364, 110642.

Hirsch, C. 2007. Fundamentals of Computational Fluid Dynamics Second edition. Elsevier's Science & Technology Rights Department, Oxford, UK.

Hyvärinen, J., Telkkä, J., & Tielinen, K. March 6 - 11, 2022. MOTEL–SMR Integral PWR System Test Facility–Design and First Test Results. Proceedings of the 19th International Topical Meeting on Nuclear Reactor Thermal Hydraulics (NURETH-19), Brussels, Belgium.

IAEA 2020. Advances in Small Modular Reactor Technology Developments. website: https://aris.iaea.org/Publications/SMR_Book_2020.pdf.

Jaffar N., Inayat M. H., Wardag A. N. K. 2017. Design a helical coil heat exchanger via CFD simulations. 2017 14th International Bhurban Conference on Applied Sciences and Technology (IBCAST), Islamabad, Pakistan.

Jawerth, N. 2020. What is the Clean Energy Transition and How Does Nuclear Power Fit In? IAEA, website: https://www.iaea.org/bulletin/what-is-the-clean-energy-transition-and-how-does-nuclear-power-fit-in.

Kilchanov, S. 2022. MOTEL facility modeling with TRACE code. LUT School of Energy Systems, website: https://lutpub.lut.fi/handle/10024/164977.

Kim K. W. et al. 2021. Numerical study on the interaction between the internal and surface waves by a 2D hydrofoil moving in two-layer stratified fluid. Proceedings of the Institution of Mechanical Engineers, Part M: Journal of Engineering for the Maritime Environment. 235(2), 480-490.

Lai J. K. et al. 2016. Large Eddy Simulations for a Helical Coil Steam Generator. Transactions of the American Nuclear Society, 155. Website: https://www.osti.gov/biblio/23042924.

Liu, H. et al. 2020. An assessment and analysis of phase change models for the simulation of vapor bubble condensation. International Journal of Heat and Mass Transfer. 157, 119924.

Modro S. M. et al. 2003. Multi-Application Small Light Water Reactor Final Report. (No. INEEL/EXT-04-01626). Idaho National Lab.(INL), Idaho Falls, ID (United States); Oregon State University, Corvallis, OR; NEXANT, Inc., San Francisco, CA (US).

Moon J. H. et al. 2022. Numerical study on subcooled water jet impingement cooling on superheated surfaces. Case Studies in Thermal Engineering. 32, 101883.

Ranjbar S. F., Seyyedvalilu M. H. 2014. The effect of geometrical parameters on heat transfer coefficient in helical double tube exchangers. Journal of Heat and Mass Transfer Research, 1(2), 75-82.

Ren Y. et al. 2018. Numerical study on pool-side saturated boiling heat transfer in spiral wound heat exchanger. Applied Thermal Engineering, 140, 657-670.

Rennie T. J., Raghavan G. S. V. 2002. Laminar parallel flow in a tube-in-tube helical heat exchange. AIC2002 Meeting CSAE/SCGR Program, Saskatchwan.

Reyes Jr J. N. 2012. NuScale Plant Safety in Response to Extreme Events. Nuclear Technology, 178(2), 153-163.

Sadrehaghighi, I. 2018. Turbulence Modeling with case studies. Annapolis MD

SANCHEZ-ESPINOZA, V., Suikkanen, H., & Valtavirta, V. 2021. Status of the H2020 McSAFER Project-Experimental and analytical investigations for the safety evaluation of water-cooled SMRs (No. IAEA-CN--308).

Telkkä, J., Suikkanen, H., Kotro, E. & Räsänen, A. 2022. SMR Experiments with the MOTEL Test Facility within the Euratom Project McSAFER.

Telkkä, J. 2018. Modular Test Loop (MOTEL). LUT University Nuclear Engineering. Lappeenranta, Findland.

Tielinen, K. et al. 2021. MOTEL facility description. Technical Report LUT University.

WILCOX, D. C. 2006. Turbulence Modeling for CFD, 3rd edition. La Canada, CA: DCW industries.

World Nuclear Association. 2023. Small Nuclear Power Reactors. Atw. Internationale Zeitschrift fuer Kernenergie, 48(2), 102-104.

Wu J. et al. 2022. Two-phase secondary flow characteristics and heat transfer mechanism during boiling in a vertical helically coiled tube. International Communications in Heat and Mass Transfer, 138, 106398.

Wu J. et al. 2022. Numerical simulation research on two-phase flow boiling heat transfer in helically coiled tube. Nuclear Engineering and Design 395, 111827, journal homepage: www.elsevier.com/locate/nucengdes.

Yuan, H. et al. 2017. Flow-induced vibration analysis of a helical coil steam generator experiment using large eddy simulation. Nuclear Engineering and Design, 322, 547-562.

Appendices

Appendix 1. The UDF code

When defining a mass transfer boundary condition for the phase change between a liquid and gas phase in a simulation, the DEFINE_MASS_TRANSFER UDF is utilized. Below, some part of the code is provided.

```
DEFINE_MASS_TRANSFER(liq_gas_source, c, t, from_index, from_species_index, to_index, to_species_index)
{
    real m_lg = 0.;
    real T = C_T(c, t);
    real p = C_P(c, t);

    Thread* gas = THREAD_SUB_THREAD(t, from_index);
    real vf_gas = C_VOF(c, gas); // Vapor volume fraction

    /* Vapor properties calculation as a function of T */
    double rho_v = get_prop_from_lut_vap(T, 0);
    double h_v = get_prop_from_lut_vap(T, 3);
    double cp_v = get_prop_from_lut_vap(T, 2);

    /* Saturated properties calculation */
    double Tsat = calc_Tsat(p); // Saturated temperature at p

    /* Liquid properties calculation as a function of T and p */
    double rho_l = get_prop_from_lut_liq(T, 0);
    double h_l = get_prop_from_lut_liq(T, 3);
    double cp_l = get_prop_from_lut_liq(T, 2);

    /* Mixture properties calculation */
    double rho_m = vf_gas * rho_v + (1. - vf_gas) * rho_l; // Mixture density
    double mf_gas = vf_gas * rho_v / rho_m; // Vapor mass fraction
    double h_fg = h_v - h_l; // Latent heat

    if (T < Tsat && mf_gas > 0)
    {
        // Calculation of the interfacial mass transfer
        double dH_max = 0.1 * fabs(cp_v * (T - Tsat) * (mf_gas * rho_m) / dt); // Heat transfer limiting function
        m_lg = dH_max / h_fg;
    }
    else if (T > Tsat && mf_gas < 1)
    {
        double dH_max = 0.1 * fabs(cp_l * (T - Tsat) * ((1. - mf_gas) * rho_m) / dt); // Heat transfer limiting function
        m_lg = -dH_max / h_fg;
    }

    return (m_lg);
}
```

DEFINE_MASS_TRANSFER takes various arguments, including the source term liq_gas_source, cell c, thread t, indices for species, and indices for source and target phases.

This UDF is an essential part of a CFD simulation model, allowing for the modelling of mass transfer during phase change (evaporation-condensation) between liquid and gas phases.